

Chapter 1

Introduction

1.1 Brief history of ISFET

The ISFET as a sensor technology with potential versatility and broad application was recognized in the mid 1970s, first described by Bergveld in the early 1970s [1]. Advanced development of theory, technology, and practical applications were done simultaneously. In addition to pH, ISFET sensor prototypes demonstrated the capability of other than available ion-selective electrodes. ISFET sensor prototypes were demonstrated for potassium, calcium, sodium, ammonium, and fluoride ions. In 1971, Professor Matsuo [2-3] conducted research on a high-impedance circuit using an organic microelectrode with an FET which proposed a measurement system employing the reference electrode. In 1978, an ISFET on a silicon island isolated by a P-N junction and insulator was proposed [1]. The discovery of the planar ISFET has been a revolutionary development for researchers previously restricted by the need for an insulating coating on the silicon substrate.

The ISFET innovation of a generally applicable discrete sensor technology for different electrochemical sensors of micrometer dimensions was realized by 1980. IC-based ISFET electrode sensors with micrometer dimensions and physical ruggedness were previously unavailable with other electrode technologies had been demonstrated. Those variables detected using potentiometric ion-selective electrode sensor systems had been fabricated and demonstrated as ISFET sensors. Multisensory probes had been designed and fabricated. Technical progress occurred at several centers in the United States, Europe, and Japan. In certain settings, the multidisciplinary nature of this

innovative sensor technology benefited from electrochemistry, bioengineering, and medical collaboration. Designs of practical ISFET sensor systems were developed, fabricated, and tested for clinically relevant applications. [4]

1.2 The evolution of the double layer model to ISFET

It was recognized that there is a direct relation between the sensitivity of the ISFET and the charging behavior of metal oxides; the metal oxides always are used to be the sensing films of the ISFET. For a long period, the site-binding model (also called site-dissociation model) developed by Yates [5] was used to describe the ISFET pH sensitivity [6]. The site-binding model, illustrated in Figure 1-1, is indicated that reactions can happen between protons (H^+) in the solution and the hydroxyl groups formed at the oxide-solution interface. At chapter 2 will briefly derived the intrinsic buffer capacity, β_s at the site-binding model which is the important factor of the ISFET sensitivity.

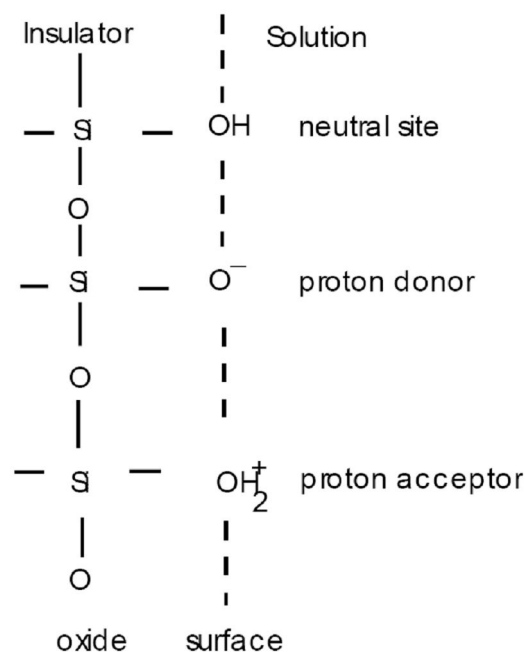


Figure 1-1 Schematic representation of the site-binding model [5]

However, the most supported model for the ISFET pH sensitivity, a combination of a double layer model with a model describes the adsorption of protons. This is an approach, which will be used to develop a new, more general model for the ISFET sensitivity. This new model can incorporate any combination of a double layer model and a charging mechanism described by surface reaction.

One of the first principals which we must be recognized is that matter at the boundary of two phases possesses properties which differentiate it from matter freely extended in either of the continuous phases which are separated by the interface. When we are talking about such a solid-solution interface, it is perhaps easier to visualize a difference between the interface and the solid than it is to visualize a difference between the interface and the extended liquid phase. Where we have a charged surface, however, there must be a balancing counter charge, and this counter charge will occur in the liquid. The charges will not be uniformly distributed throughout the liquid phase, but will be concentrated near the charged surface. Thus, we have a small but finite volume of the liquid phase which is different from the extended liquid. There are several models to describe the double layer capacitor in next section.

1.2.1 Helmholtz Double Layer

This theory is based on two concentric spheres. In 1850's, the double layer structure for the metal-electrolyte interface was first supported by Helmholtz. He took the double layer as a parallel capacitor, illustrated in Figure 1-2(a), The Helmholtz layer is divided into two plane, one is inner Helmholtz plane which is dehydrated ions immediately next to a surface and the other is outer Helmholtz plane at the center of a next layer of hydrated. The capacitor between the inner and outer Helmholtz plane is the double layer

capacitor C_s which depend on the surface potential which is contributed by the ions of the aqueous solution. The double layer capacitor is not a constant which follow the concentration of electrolyte. In Fig. 1-2(b), we can obtain the relation between the surface potential and the bulk potential is linear. As the concentration of electrolyte is very high, the Helmholtz double layer model is suitable for use, otherwise it can not been applied. The Helmholtz theoretical treatment does not adequately explain the behavior of charged colloids in suspension, however, since it hypothesizes rigid layers of opposite charges. This does not occur in nature.

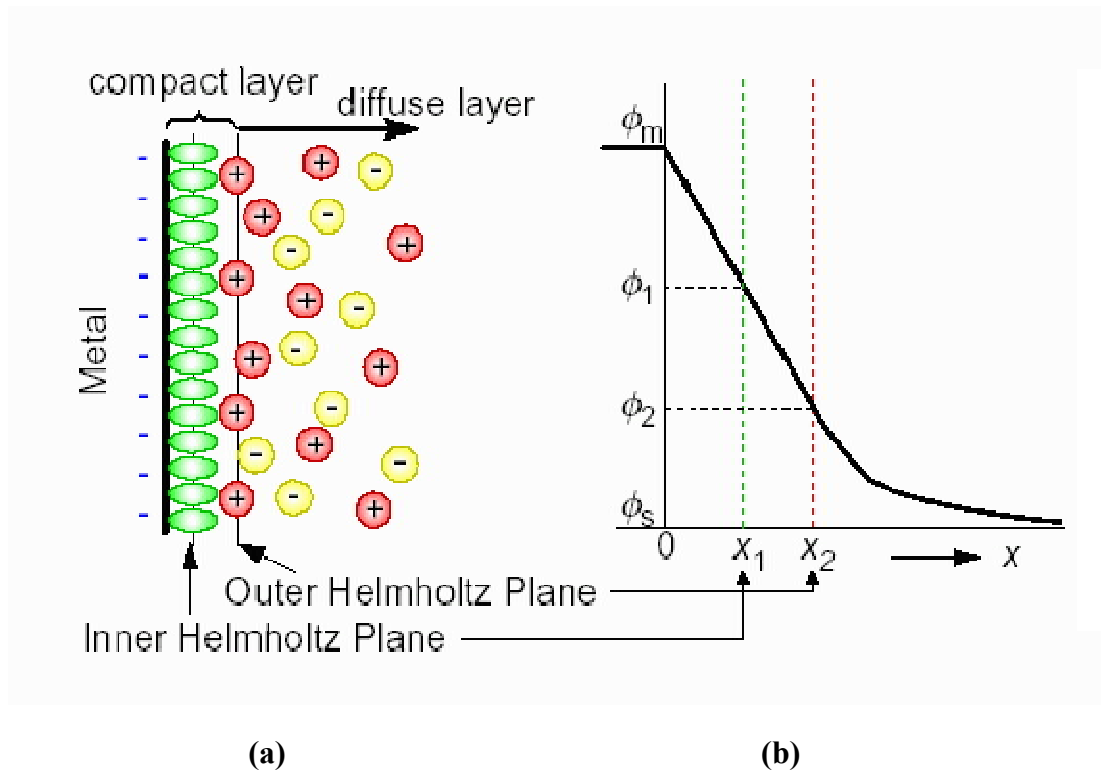


Figure 1-2 Schematic representation of the Helmholtz double layer model (a) The charge distribution, (b) The potential distribution [7]

1.2.2 Gouy-Chapman Double Layer

The Gouy-Chapman theory describes a rigid charged surface, with a cloud of

oppositely charged ions in the solution, the concentration of the oppositely charged ions decreasing with distance from the surface. This is the so-called diffuse double layer. The Helmholtz double layer model only considered the electrostatics force but ignore the thermal motion among the ions, so that it can not explain the value of the double layer capacitor, and the relation between the surface potential and the concentration of electrolyte which depend on each other. In the beginning of twenty century Gouy and Chapman proposed independently the idea layer to interpret the capacitive behavior of an electrode-electrolyte solution interface.

Gouy and Chapman thought it was impossible that the ions were fixed at the metal-electrolyte interface regularly. The electrostatics force among electrode and ions, besides there is also an molecular thermal motion effect on the ions that makes a part of ions disperse near the bulk solution. As a result, the Gouy and Chapman model [8] was proposed to adjust the Helmholtz double layer model.

This theory is still not entirely accurate. Experimentally, the double layer thickness is generally found to be somewhat greater than calculated. The error becomes greater in a dilute solution containing highly charged colloids. This assumption causes unrealistic high concentrations of ions near the surface at high value of surface potential. An adjustment to solve this problem was first suggested by Stern [9].

1.2.3 Stern Modification of the Diffuse double Layer

The Gouy-Chapman theory provides a better approximation of reality than does the Helmholtz theory, but it still has limited quantitative application. Stern, therefore, modified the Gouy-Chapman diffuse double layer in 1924. His theory states that ions do have finite size, so cannot approach the surface closer than a few nm. The first ions of the Gouy-Chapman Diffuse Double Layer are not at the surface, but at some distance δ away

from the surface. As a result, the potential and concentration of the diffuse part of the layer is low enough to justify treating the ions as point charges. Stern obtain if the concentration of electrolyte was high that the Helmholtz double layer model could match the experiment, but the concentration of electrolyte was not high enough the Gouy and Chapman model was suitable to use.

Stern also assumed that it is possible that some of the ions are specifically adsorbed by the surface in the plane δ , and this layer has become known as the Stern Layer. Therefore, the potential will drop by $\Psi_0 - \Psi_\delta$ over the "molecular condenser" (ie. the Helmholtz Plane) and by Ψ_δ over the diffuse layer. Ψ_δ has become known as the zeta (ζ) potential. This new model is called the Gouy-Chapman-Stern model, shown in Figure 1-4 illustrates. The Gouy-Chapman-Stern model involves two parts:

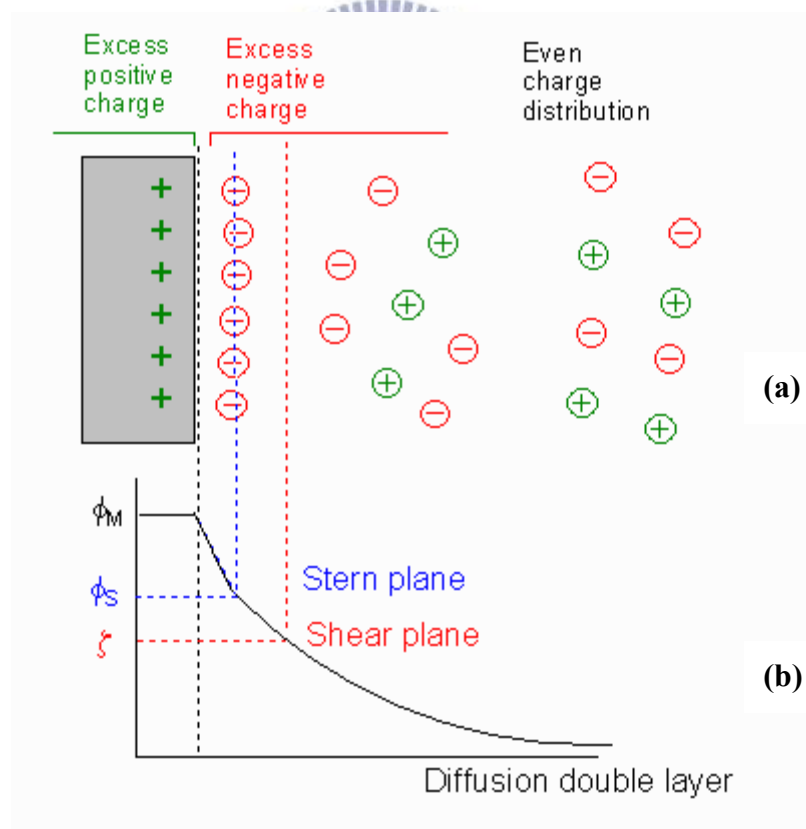


Figure 1-3 Schematic representation of Gouy – Chapman – Stern model (a) The charge distribution, (b) The potential distribution [7]

(1) The front part is stern layer which obey the Helmholtz double layer, the thickness d from the metal-electrolyte interface is nearly to the electrolyte ions radius, the great part of ions are included in the Stern layer.

(2) The later part is diffuse layer which contain remnant electrolyte ions, the ions decay according to the Gouy and Chapman model in this layer. The surface potential to the bulk solution is the sun of the stern layer and the diffuse layer, and the double layer capacitor is series connection by the stern capacitor and the diffuse capacitor.

1.3 Introduction to ISFET

ISFET-based biosensors are energetically studied by many groups because of their attractive features such as small size, low-cost, and there are multiple integrations of biologically active materials (e.g., enzymes, antibodies, DNA, and cells). ISFET was proposed by Bergveld more than 30 years ago, more than 600 papers appeared in these 30 years devoted on ISFETs and another 150 on related devices [10]. By the way , the pH-ISFTE can be not only a chemical sensor but also a physical sensor [11]. Instead, The ISFET can be a multi-senor to measure the flow-velocity, flow-direction and diffusion-coefficient.

Traditional chemical analysis can not be the usual instrument, because of the size and even the coat that can not be the personal chemical analysis. The ISFET has advantages over than ion selective electrode (ISE), such as small size, low coat and robustness. In spite of ISFET have proposed more 30 years, there are less product in the market, the main problem is that ISFET has only sensing layer in its gate region which contact the aqueous solution. By contrast, in a CMOS process poly-Si electrode in the gate region is required to define the self-aligned source and drain regions for the MOS transistors. This means that specific processes or design structures must be used to

fabricate the ISFETs in a CMOS process. The fabrication of pH-sensitivity ISFET devices in an undefined two-metal commercial CMOS technology is reported by J.Bausells [12].

1.4 Introduction to SPE (screen-printed electrode)

Over the past years, various fabrication methods have been proposed for producing planar-form, solid electrolyte modified reference electrodes of different types. Since disposable sensors hold a clear advantage for on-site testing, The screen-printed silver electrode strip (SP-AgES) has been reported. The proposed sensor strip is fabricated simply by screen-printing silver ink onto a polypropylene (PP) base with Ag-working, Ag-counter and Ag/Ag_xO reference electrodes. Silver electrodes have been reported to have the best electrocatalytic activity with an appropriate choice of supporting electrolyte in halide analysis. The use of Ag ink pseudo-reference electrode (i.e., Ag⁺/0) is not suitable for the strip since at ambient conditions Ag can be easily converted to its oxides. The subsequent chlorination of Ag ink in the detection of chloride ion may also induce the formation Ag/AgCl and hence a potential shift. The planar and fully screen-printed SP-AgES and its analytical utilities are demonstrated especially on the stability and reproducibility of the Ag/Ag_xO reference electrode [13]. The main advantages of SPE are low price, flexible design, easy produce, rugged, portable and easy to clean.

1.5 Motivation of this work

ISFET has been established complete theory and technique, and developed many applications such as ISFET-based biosensor. There are still needs many developments in ISFET, for example, new materials of sensing membranes, fabrication process and

surface modification. We would like to study ISFET by EIS capacitor, and analyze ZrO_2 high-k materials as sensing film by the sol-gel method. Following descriptions are major motivation in our study:

- a. In our lab, the sol-gel process has been studied for a long time. We want to increase the applications of sol-gel-derived materials, and understand much more characteristics of high-k materials.
- b. We try to make EIS capacitors to study the sensing characters of ZrO_2 , simplify fabrication process and decrease the cost of production.
- c. Screen-printed electrode is a convenient substrate for extending gate of EIS capacitor and make solid-state reference electrode. When we measure the pH sensitivity by Capacitance-Voltage measurement, we can just immerse the sensing range of EIS capacitor in pH buffer solution to do fast and synchronous test.
- d. In human organism, as urea is a final product of protein metabolism, its accumulation above critical levels must be carefully determined. So, urea monitoring is of great interest in clinical and biomedical analysis because this biomolecule enables the diagnosis of some diseases such as kidney and liver malfunction, and also make possible to predict the nature and causes of diabetes [14–16]. Urea is also related to other processes such as soil fertilization, in which it acts as a nitrogen source for plants. For the purpose of urea sensing, various procedures are applied and interesting results have been obtained with enzyme-based sensors. The incorporation of a biological moiety (enzymes, cells, antigens, DNA) to a conventional physico-chemical transducer characterizes a biosensor, and the presence of the biomolecule provides a high specificity to biosensors. We study the urea sensitivity of ZrO_2 EIS capacitor and immobilization of urease.

The following flowchart is the total process of our study as shown in figure 1-4. The parameters of experiment are also described, and the red items are better parameters.

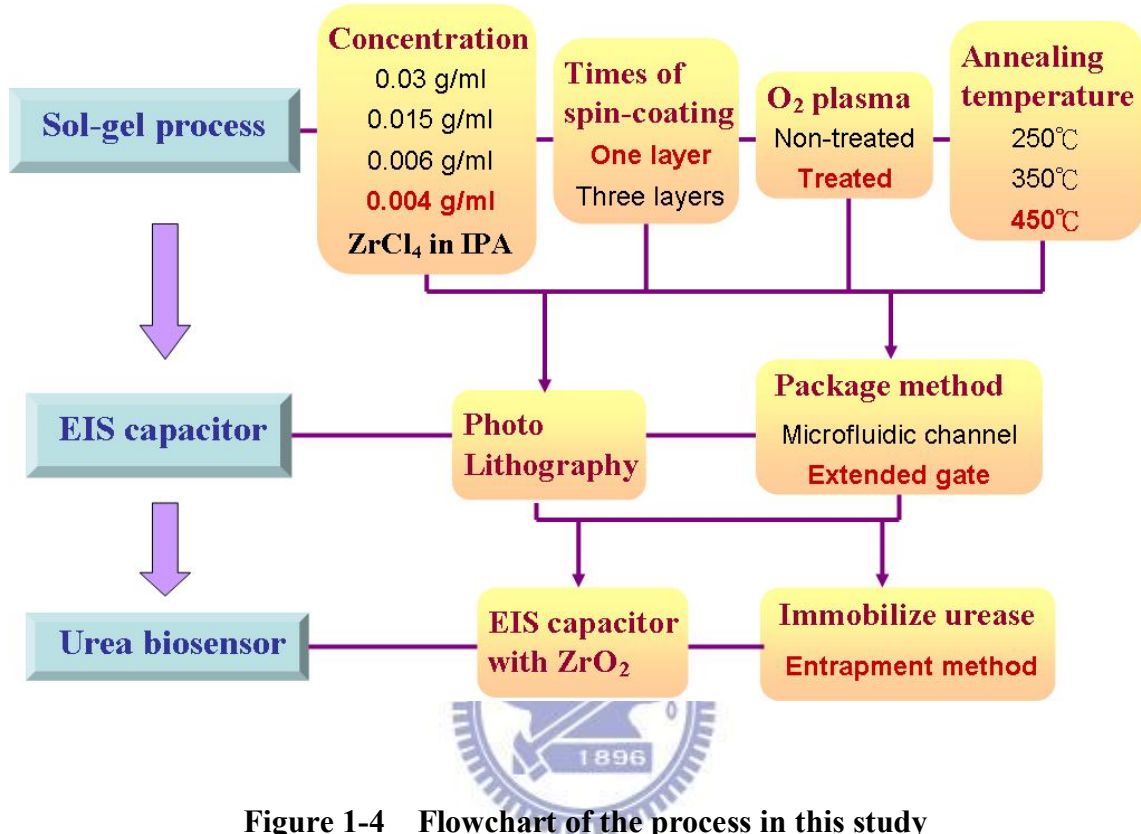


Figure 1-4 Flowchart of the process in this study

1.6 References

- [1] P. Bergveld, Development of an ion sensitive solid-state device for neurophysiological measurements, IEEE Transactions on Bio-Medical Engineering 17 (1970) 70.
- [2] T. Matsuo, K. D. Wise, An integrated field-effect electrode for biopotential recording, IEEE Transactions on Bio-Medical Engineering 21 (1974) 485.
- [3] T. Matsuo, M. Esashi, Method of ISFET fabrication, Sensors and Actuators B 1 (1982) 77.
- [4] B. A. McKinley, ISFET and Fiber Optic Sensor Technologies: In Vivo Experience for

Critical Care Monitoring, Chemical Reviews 108 (2008) 826-844.

[5] D. E. Yates, S. Levine, T. W. Healy, Site-binding model of the electrical double layer at the oxide/water interface, Journal of the Chemical Society-Faraday Transactions I 70 (1974) 1807-1818.

[6] L. Bousse, N. F. De Rooij, P. Bergveld, Operation of chemically sensitive field-effect sensors as a function of the insulator-electrolyte interface, IEEE Transactions on Electron Devices 30 (1983) 1263-1270.

[7] P. Atkins, J. de Paula, W. H. Freeman, Physical Chemistry 8th, Oxford (2007).

[8] R. E. G. van Hal, J. C. T. Eijkel, P. Bergveld, A general model to describe the electrostatic potential at electrolyte oxide interfaces, Advances in Colloid and Interface Science 69 (1996) 31-62.

[9] O. Stern, Zur Theorie der, Elektrolytischen Doppelschicht, Electrochemistry 30 (1924) 508.

[10] P. Bergveld, Thirty years of ISFETOLOGY what happened in the past 30 years and what may happen in the next 30 years, Sensors and Actuators B 88 (2003) 1-20.

[11] A. Poghosian, L. Berndsen, M. J. Schöning, Chemical sensor as physical sensor: ISFET-based flow-velocity, Sensors and Actuators B 95 (2003) 384-390.

[12] J. Bausells, J. Carrabina, A. Errachid, A. Merlos, Ion-sensitive field-effect transistors fabricated in a commercial MOS technology, Sensors and Actuators B 57 (1999) 56-62.

[13] M. H. Chiu, W. L. Cheng, G. Muthuraman, C. T. Hsu, H. H. Chung, J. M. Zen, A disposable screen-printed silver strip sensor for single drop analysis of halide in biological samples, Biosensors and Bioelectronics 24 (2009) 3008-3013.

[14] V. Rajesh, W. Bisht, K. Takashima, Kaneto, An amperometric urea biosensor based on covalent immobilization of urease onto an electrochemically prepared copolymer poly (*N*-3-aminopropyl pyrrole-co-pyrrole) film, Biomaterials 26 (2005) 3683-3690.

[15] R. Sahney, S. Anand, B. K. Puri, A. K. Srivastava, A comparative study of immobilization techniques for urease on glass-pH-electrode and its application in urea detection in blood serum, *Analytica Chimica ACTA* 578 (2006) 156–161.

[16] F. Kuralay, H. Ozyoruk, A. Yildiz, Amperometric enzyme electrode for urea determination using immobilized urease in poly(vinylferrocenium) film, *Sensors and Actuators B* 114 (2006) 500–506.



Chapter 2

Theory Description

2.1 Introduction

This chapter will define and explain the theories of ISFET which are relevant to metal oxide semiconductor field effect transistor (MOSFET) and drift mechanism will be interpreted in turn. In the first section will describe what pH is briefly. Subsequently, the theory of ISFET includes both ISFET concept and the relation between oxide to electrolyte interface. Then make a description of the sol-gel processes and application in ISFET fabrication. The non-ideal phenomena of ISFET: Optical effect, Hysteresis, Drift and Lifetime, will be explained In the final section.



2.2 Importance of Ion-sensitivity

- a. Measuring pH is essential in finding the chemical characteristics of a substance. Both the solubility of many chemicals or bimolecular in solution and the speed or rate of (bio-)chemical reactions are dependent on pH.
- b. The body fluid of living organisms usually has specific pH range. Soil pH affects the livability of plants and it is important in farming. The wastewater from factories and households may cause the pH changes of water and brings the environmental impact on the local or even remote inhabitants. [1]
- c. Electrolytic balance is very important in organisms. For example, calcium is the one mineral that can really alkalize your body. It produces the calcium buffering compound Mono-ortho-calcium phosphate which raises your pH.

2.3 Definition of pH

The term pH is derived from a combination of p for the word power and H for the symbol of the element hydrogen [2]. In aqueous solution, the following equilibrium exists between the water (H₂O), the acid (H⁺) and the alkali (OH⁻):



pH is one of the most common chemical and biomedical measurements. The degree of the pH is the solution of ionization which can supply how much hydrogen ions (H⁺), not the concentration of the solution itself. The definition in pH is expressed as

$$pH = -\log a_{\text{H}^+} = -\log \gamma[\text{H}^+] \quad (2-2)$$

where a_{H^+} is the hydrogen ion activity, γ is the activity coefficient which equals to 1 when diluted solution, and $[\text{H}^+]$ is the molar concentration of solvated protons in units of moles per liter. In practice, pH depends on a number of factors, such as the concentration of the added acid and its dissociation constant [3].

2.4 The detection methods for pH

Traditionally, the methods for the measurement of pH values include indicator reagent, pH test strips, metal electrode and glass electrode. There are some drawbacks on the other methods, except for glass electrode. Such as, indicator reagent can show different colors at different solvent, but it only exhibit a range of pH not the accuracy value; As pH test strips immersed in the test liquid, they show a particular color corresponding to the pH of the solution. These are similar to indicator reagent; The hydrogen electrode method is a golden standard for all methods of pH measure. The

activity of the hydrogen ions is determined by potentiometric measurement using a standard hydrogen electrode and a reference electrode. In order to ensure a saturated layer of hydrogen adsorbed at the platinum surface, hydrogen gas is continuously bubbled around the platinum electrode. However, this method is not suitable for daily use due to the inconvenience of handling hydrogen gas [2]. Because of some limitations in practical applications of the first three methods, the glass electrode becomes the most widely used method for the pH measurement, and it is considered to be the standard measuring method.

The glass electrode is most widely used for pH measurement due to ideal Nernstian response independent of redox interferences, short balancing time of electrical potential, high reproducibility and long lifetime. However, glass electrode has several drawbacks for many industrial applications. Firstly, they are unstable in alkaline or HF solutions or at temperatures higher than 100°C. Also, they exhibit a sluggish response and are difficult to miniaturize. Moreover, they cannot be used in food or in vivo applications due to their brittle nature [1]. There is an increasing demand for alternative pH electrodes [2].

New trends of pH measurements such as optical-fiber-based pH sensor, mass-sensitive pH sensor, metal oxide sensor, conducting polymer pH sensor, nano-constructed cantilever-based pH sensor, ISFET-based pH sensor and pH-imaging sensor. In this study, we will discuss what problems in practical applications of ISFETs and how to improve them.

2.5 The theory of ISFET

Electrochemical measurement of pH utilizes devices that transduce the chemical activity of the hydrogen ion into an electronic signal, such as an electrical potential difference or a change in electrical conductance. Since ISFET was the first reported by

Bergveld, research on new material of sensing thin and fabrication process to improve the sensitivity and stability has been continuously proposed [5-7]. At the same time, the mechanism of the pH response of pH ISFET has also been studied extensively [6-12]. The followings are the theoretical foundations which are mostly adopted to characterize the ISFET.

2.5.1 From MOSFET to ISFET

Because the structures are similar, the basic operational mechanisms are alike. At Figure 2-2 illustrates, it can observe the similarities and differences between MOSFET and ISFET.

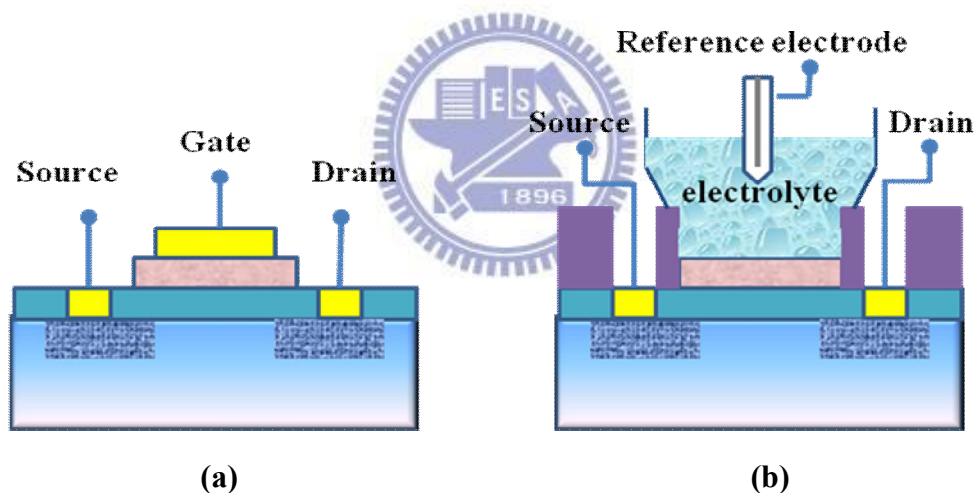
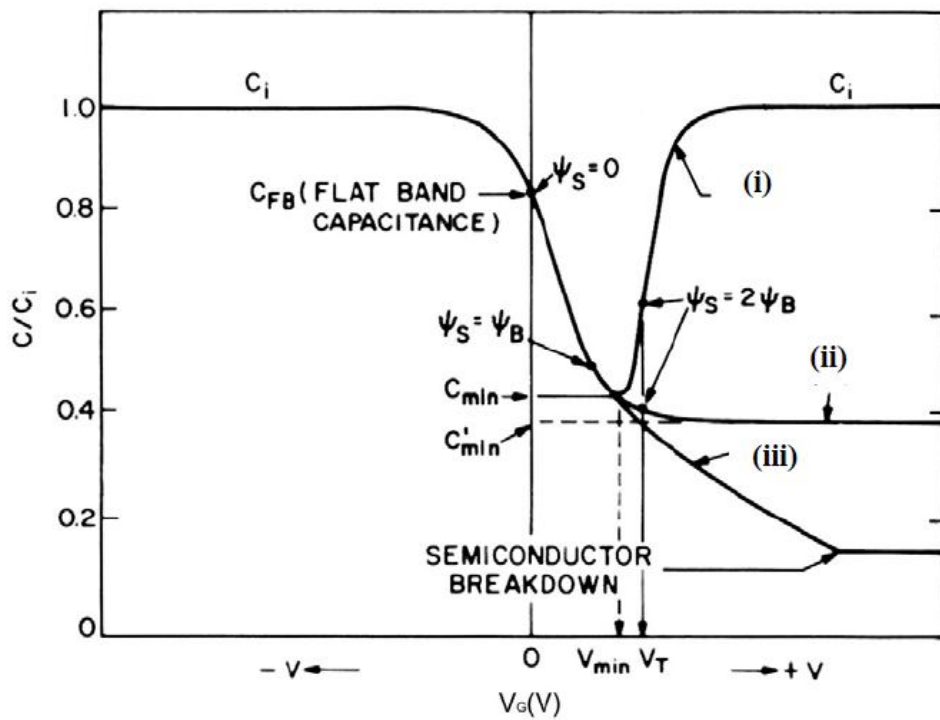


Figure 2-1 Schematic representation of (a) MOSFET, (b) ISFET

The ISFET is a new approach of electrochemical measurement of pH, which is similar to MOSFET except that the metal/poly gate is replaced by sensing layers, and the sensing layer is immersed in aqueous solution. Because of it can not directly supply on the aqueous, therefore the reference electrode is adopted to connect with sensing layer. The reference electrode not only supply stable voltage but also can connect the circuit with sensing layer to make a loop. It can trace back to the history of the development of

ISFET, it is not difficult to find out the similarities between ISFET and MOSFET. In general MOSFET is Metal-Insulator-Semiconductor structure, ISFET is Electrolyte-Insulator-Semiconductor structure. The most obvious characteristic is the similarity between their structures. For this reason, the best way to comprehend the ISFET is to understand the operating principle of a MOSFET first. Figure 2-2 shows C-V characters and the charge distribution of an ideal MIS capacitor.



(a)

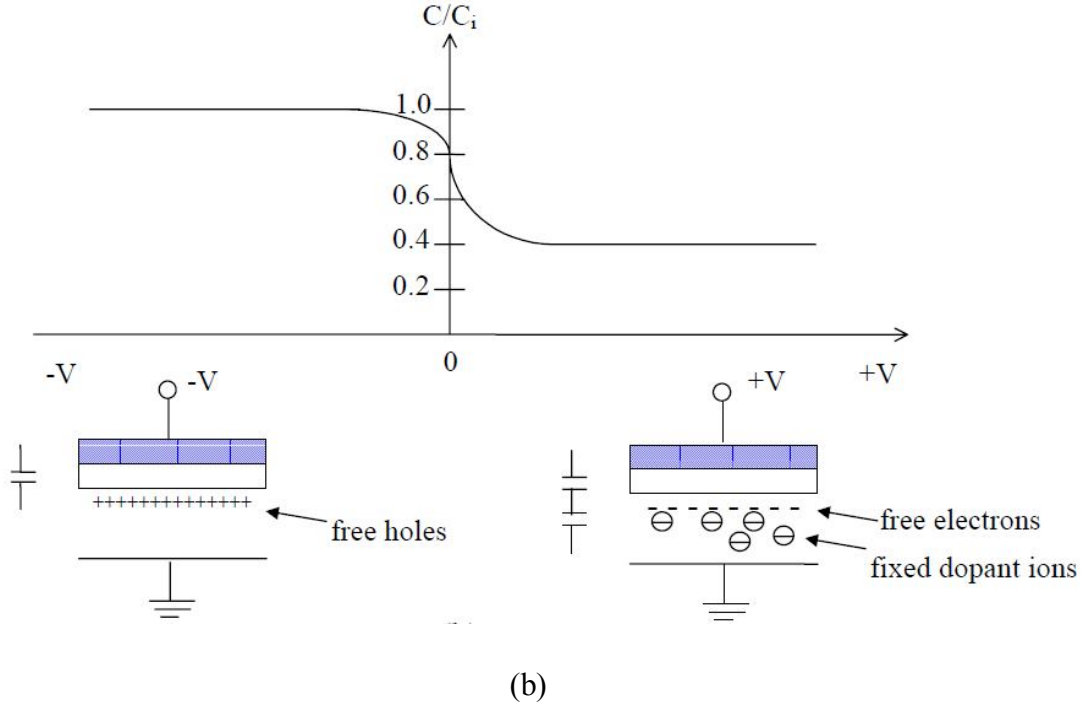


Figure 2-2 C-V characters of an ideal MIS capacitor (a) C-V curves of an MIS structure, (b) The charge distribution of an MIS capacitor [13]

When MOSFET is operated in the so-called ohmic or non-saturated region, the drain current I_D is given by:

$$I_D = \frac{C_{OX}\mu W}{L} \left\{ (V_{GS} - V_T) - \frac{1}{2}V_{DS} \right\} V_{DS} \quad (2-3)$$

where C_{OX} is the gate insulator capacitor per unit area; μ is the electron mobility in the channel; W/L is the width-to-length ratio of the channel; V_{GS} is gate to source voltage; V_{DS} is drain to source voltage and V_T is the threshold voltage. V_T can be described by following expression:

$$V_T = V_{FB} - \frac{Q_B}{C_{OX}} + 2\phi_F \quad (2-4)$$

where V_{FB} is the flat-band voltage; Q_B is the depletion charge in the silicon substrate, and ϕ_F is the potential difference between the Fermi level and intrinsic Fermi level. The degree of ϕ_F is dependent on the doped concentration. V_{FB} can be described by following expression:

$$V_{FB} = \frac{\Phi_M - \Phi_{Si}}{q} - \frac{Q_{OX} + Q_{SS}}{C_{OX}} \quad (2-5)$$

where Φ_M is the work function of the gate metal; Φ_{Si} is the work function of silicon; Q_{OX} is the charge in the oxide and Q_{SS} is the surface state density at the oxide-silicon interface. Substitution of Eq. (2-4) in Eq. (2-5), the general form of the threshold voltage of a MOSFET can be described by following expression:

$$V_T = \frac{\Phi_M - \Phi_{Si}}{q} - \frac{Q_{OX} + Q_{SS} + Q_B}{C_{OX}} + 2\phi_F \quad (2-6)$$

In the case of ISFET, the metallic gate is taken off. So that, the term Φ_M and Φ_{Si} are no longer to be considered on the ISFET. When immersed in an aqueous solution, it must occur surface potential at the oxide-solution interface. The surface potential must be taken into account. Hence the threshold voltage becomes the following expression:

$$V_T = E_{ref} + \chi^{sol} - \psi_0 - \frac{\Phi_{Si}}{q} - \frac{Q_{OX} + Q_{SS} + Q_B}{C_{OX}} + 2\phi_F \quad (2-7)$$

where E_{ref} is the constant potential of the reference electrode; χ^{sol} is the surface dipole potential of the solution which also has a constant value. The surface dipole potential is different from an aqueous solution, even though a little variation of surface dipole potential at disparity aqueous solution. The value compared to other terms is too small to be taken as a constant. All terms are constant except ψ_0 , it is the kernel of ISFET sensitivity to the electrolyte pH which is controlling the dissociation of the oxide surface. The charge density and potential distribution of the interface to EIS are shown in figure 2-3. Figure 2-4 is EIS system represented by equivalent capacitor structure.

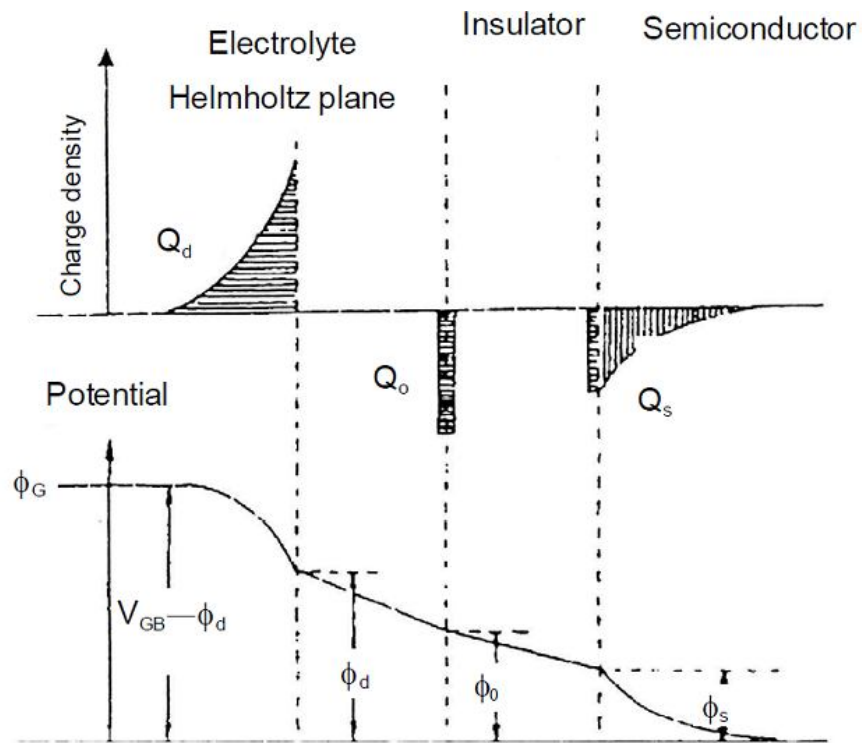
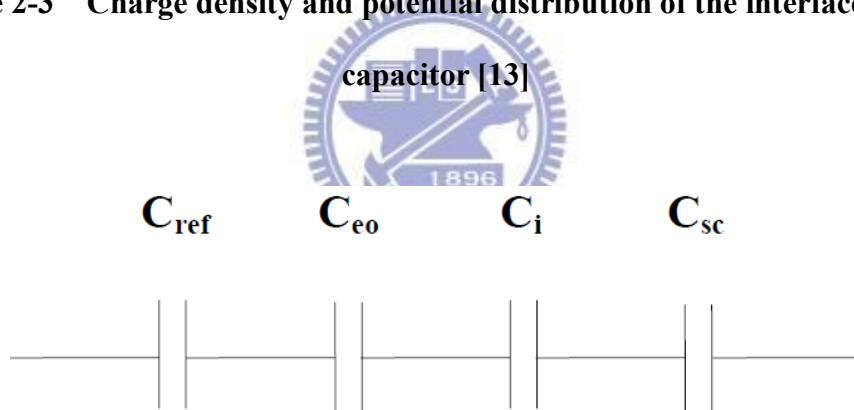


Figure 2-3 Charge density and potential distribution of the interface to EIS capacitor [13]



- C_{ref} : Reference electrode capacitance
- C_{eo} : Electrolyte/insulator capacitance
- C_i : insulator capacitance
- C_{sc} : Semiconductor space charge capacitance

Figure 2-4 EIS system represented by equivalent capacitor structure

Figure 2-5 and 2-6 are the energy band diagrams of an ideal MIS capacitor and the interface to EIS capacitor.

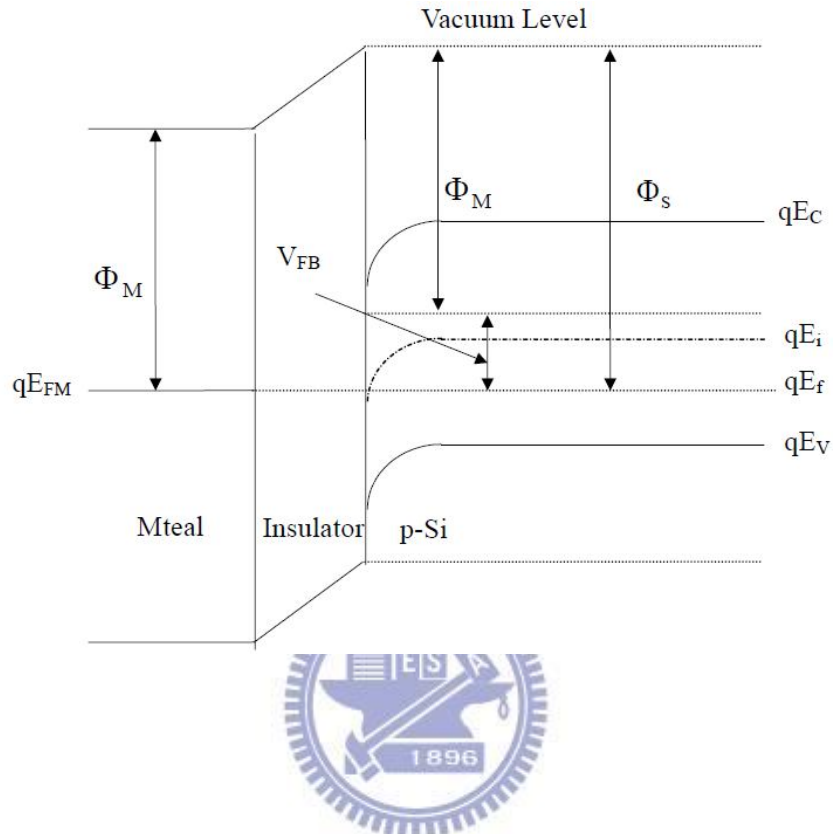


Figure 2-5 Energy band diagrams of an ideal MIS capacitor [14]

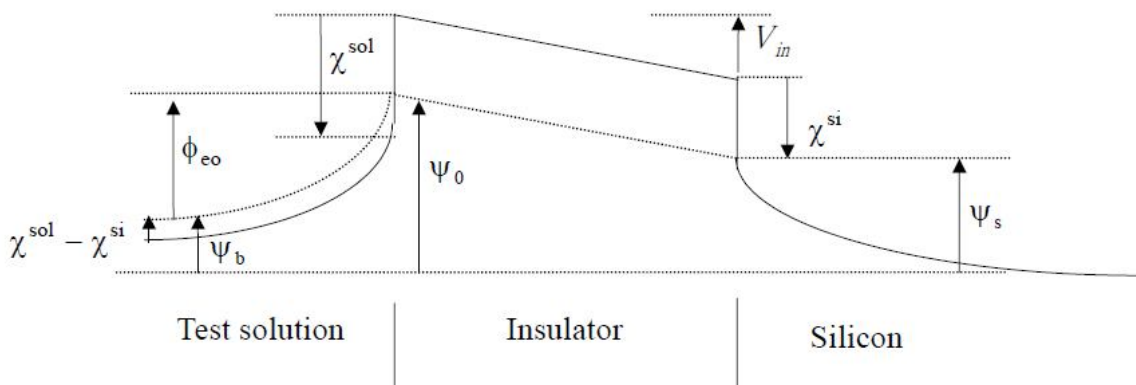


Figure 2-6 Energy band diagrams of the interface to EIS capacitor [14]

2.5.2 The Response of pH at the Oxide-Electrolyte Interface

The surface of any metal oxide always contains hydroxyl groups, in the case of silicon dioxide SiOH groups [15]. These groups consist of donate and accept a proton from the solution. Therefore, as ISFET sensing layer like SiO₂ contact an aqueous solution, the change of pH will change the SiO₂ surface potential. These reactions can be expressed by:



where H_s^+ represents the protons at the surface of the oxide.

The potential between the gate insulator surface and the electrolyte solution causes a proton concentration difference between bulk and surface that is according to

Boltzmann:

$$a_{H_s^+} = a_{H_B^+} \exp \frac{-q\Psi_0}{KT} \quad (2-10)$$

Or

$$pH_s = pH_B + \frac{q\Psi_0}{2.3KT} \quad (2-11)$$

where a_{H^+} is the activity of H⁺; q is the elementary charge; k is the Boltzmann constant and T is the absolute temperature. The subscripts B and S refer to the bulk and the surface, respectively.

There are two important parameters which are related to ISFET sensitivity, β_s and C_s . β_s is the symbol of the surface buffer capacity, the ability of β_s as the oxide surface to deliver or take up protons, and C_s is the differential double-layer capacitor, of which the value is mainly determined by the ion concentration of the bulk solution via the

corresponding Debye length.

$$\frac{\Delta\sigma_0}{\Delta pH_S} = -q\beta_S \quad (2-12)$$

where σ_0 is the surface charge per unit area. β_S is called the intrinsic buffer capacity because it is the capability to buffer small changes in the surface pH (pH_S), but not in the bulk pH (pH_B).

Because of charge neutrality, an equal but opposite charge is built up in the electrolyte solution side of the double layer σ_{DL} . This charge can be described as a function of the integral double layer capacitor, C_i , and the electrostatic potential:

$$\sigma_{DL} = -C_i\Psi_0 = -\sigma_0 \quad (2-13)$$

The integral capacitor will be used later to calculate the total response of the ISFET on changes in pH. The ability of the electrolyte solution to adjust the amount of stored charge as result of a small change in the electrostatic potential is the differential capacitor,

C_s :

$$\frac{\Delta\sigma_{DL}}{\Delta\Psi_0} = -\frac{\Delta\sigma_0}{\Delta\Psi_0} = -C_s \quad (2-14)$$

As a result, combination of Eq.(2-12) to (2-14) lead to an expression for the sensitivity of the electrostatic potential change in

a_{HS^+} :

$$\frac{\Delta\Psi_0}{\Delta pH_S} = \frac{\Delta\Psi_0}{\Delta\sigma_0} \frac{\Delta\sigma_0}{\Delta pH_S} = \frac{-q\beta_S}{C_s} = \frac{\Delta\Psi_0}{\Delta\left(pH_B + \frac{q\Psi_0}{2.3KT}\right)} \quad (2-15)$$

Rearrange Eq. 2-15 gives a general expression for the sensitivity of the electrostatic potential to changes in the bulk pH [15]:

$$\Delta\Psi_0 = -2.3\alpha \frac{KT}{q} \Delta pH_B \quad (2-16)$$

with

$$\alpha = \frac{1}{\frac{2.3KTC_s}{q^2\beta_s} + 1} \quad (2-17)$$

The parameter α is a dimensionless sensitivity parameter that varies between 0 and 1, depending on the intrinsic buffer capacity, β_s , of the oxide surface and the differential capacitor C_s . We can get the maximum value α so that the sensitivity become -59.2 mV/pH at 298K which is called Nernstian sensitivity.

Therefore, the intrinsic buffer capacity β_s need to be the more higher or the double layer capacity C_s to be the more lower. In ideal, the intrinsic buffer capacity $\beta_s = \infty$ or the double layer capacity $C_s = 0$ would be the best. It appears that the usual SiO_2 from MOSFET does not fulfill the requirements of a high value of β_s . The pH sensitivity is low depending also on the electrolyte concentration through C_s . Therefore other films such as ZrO_2 were introduced to increase the values of β_s . The higher the intrinsic buffer capacity so that the less important of the value of C_s which means that independent of the electrolyte concentration a Nernstian sensitivity can be achieved over a pH range from 1 to 13.

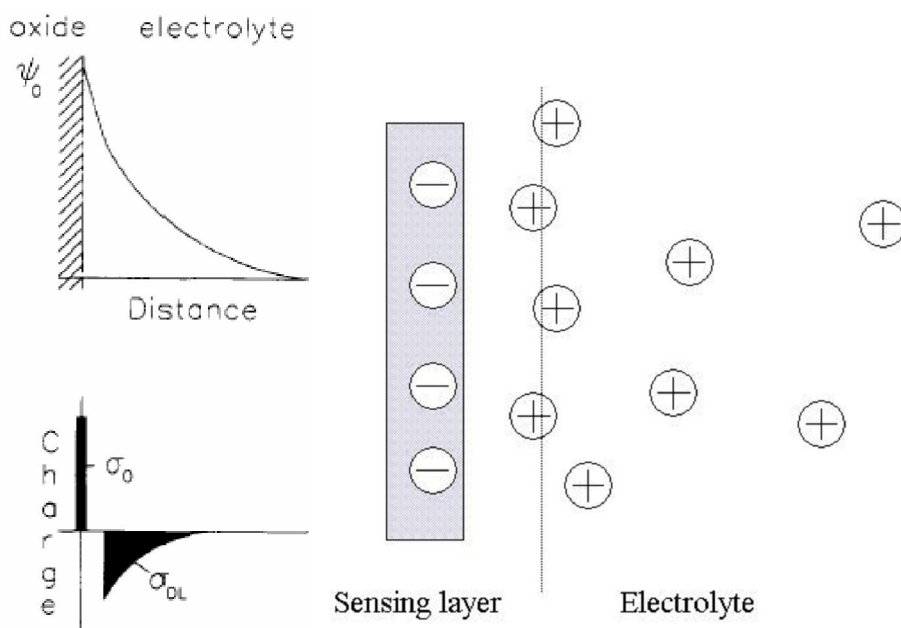


Figure 2-7 Potential profile and charge distribution at an oxide electrolyte solution interface

2.6 The mechanism of sol-gel processes

The interest in sol-gel processing can be traced back in the mid-1880s with the observation that the hydrolysis of tetraethyl orthosilicate (TEOS) under acidic conditions led to the formation of SiO₂ in the form of fibers and monoliths. The sol-gel process, also known as chemical solution deposition, is a wet-chemical technique widely used in the fields of materials science and ceramic engineering. Such methods are used primarily for the fabrication of materials (typically a metal oxide) starting from a chemical solution which acts as the precursor for an integrated network (or *gel*) of either discrete particles or network polymers. The formation of a metal oxide involves connecting the metal centers with oxo (M-O-M) or hydroxo (M-OH-M) bridges, therefore generating metal-oxo or metal-hydroxo polymers in solution. Thus, the sol evolves towards the formation of a gel-like diphasic system containing both a liquid phase and solid phase whose morphologies range from discrete particles to continuous polymer networks, a hydroxyl ion becomes attached to the silicon atom as follows:



In the case of the colloid, the volume fraction of particles (or particle density) may be so low that a significant amount of fluid may need to be removed initially for the gel-like properties to be recognized. This can be accomplished in any number of ways. The simplest method is to allow time for sedimentation to occur, and then pour off the remaining liquid. Centrifugation can also be used to accelerate the process of phase separation.

Removal of the remaining liquid (solvent) phase requires a drying process, which is typically accompanied by a significant amount of shrinkage and densification. The rate at

which the solvent can be removed is ultimately determined by the distribution of porosity in the gel. The ultimate microstructure of the final component will clearly be strongly influenced by changes imposed upon the structural template during this phase of processing. Afterwards, a thermal treatment, or firing process, is often necessary in order to favor further polycondensation and enhance mechanical properties and structural stability via final sintering, densification and grain growth. One of the distinct advantages of using this methodology as opposed to the more traditional processing techniques is that densification is often achieved at a much lower temperature.

The precursor sol can be either deposited on a substrate to form a film (e.g., by dip coating or spin coating), cast into a suitable container with the desired shape, or used to synthesize powders. The sol-gel approach is inexpensive and processing low-temperature technique that allows for the fine control of the product's chemical composition. It can be used in ceramics processing and manufacturing as an investment casting material, or as a means of producing very thin films of metal oxides for various purposes. The sol-gel derived materials have diverse applications in optics, electronics, energy, space, biosensors, medicine (e.g., controlled drug release), reactive material and chromatography technology. [16][17]

2.6.1 Application of the sol-gel processes in ISFET fabrication

The sol-gel process is a wet-chemical technique used for the fabrication of both glassy and ceramic materials. It can be used to provide flexible and precise control over the stoichiometry. The sol-gel method has drawn a considerable amount of attention in the scientific and technological fields because of its generally lower temperature processing condition, easier composition control and homogeneity, non-vacuum technique and low cost. There are many sol-gel-derived materials be applied to ISFET,

such as PbTiO_3 , BaTiO_3 and SnO_2 .

2.6.2 O_2 plasma in the sol-gel processes

Plasma is a gas in which a certain portion of the particles are ionized. The presence of a non-negligible number of charge carriers makes the plasma electrically conductive so that it responds strongly to electromagnetic fields. Plasma, therefore, has properties quite unlike those of solids, liquids, or gases and is considered to be a distinct state of matter. Like gas, plasma does not have a definite shape or a definite volume unless enclosed in a container; unlike gas, in the influence of a magnetic field, it may form structures such as filaments, beams and double layers. Plasma was first identified in a Crookes tube, and so described by Sir William Crookes in 1879 (he called it "radiant matter"). The nature of the Crookes tube "cathode ray" matter was subsequently identified by British physicist Sir Joseph John Thomson in 1897, and dubbed "plasma" by Irving Langmuir in 1928.

In this study, we detected O_2 plasma could react with "sol" more efficiently. Monodisperse powders, for example, may therefore be stabilized sufficiently to ensure a high degree of order in the colloidal crystal or polycrystalline colloidal solid which results from aggregation. Such defective polycrystalline colloidal structures would appear to be the basic elements of submicrometre colloidal materials science, and, therefore, provide the first step in developing a more rigorous understanding of the mechanisms involved in microstructural evolution in inorganic systems such as polycrystalline ceramics. The Oxygen free radicals can react with metal oxide sol in depth, as shown in Figure 2-8 illustrates.

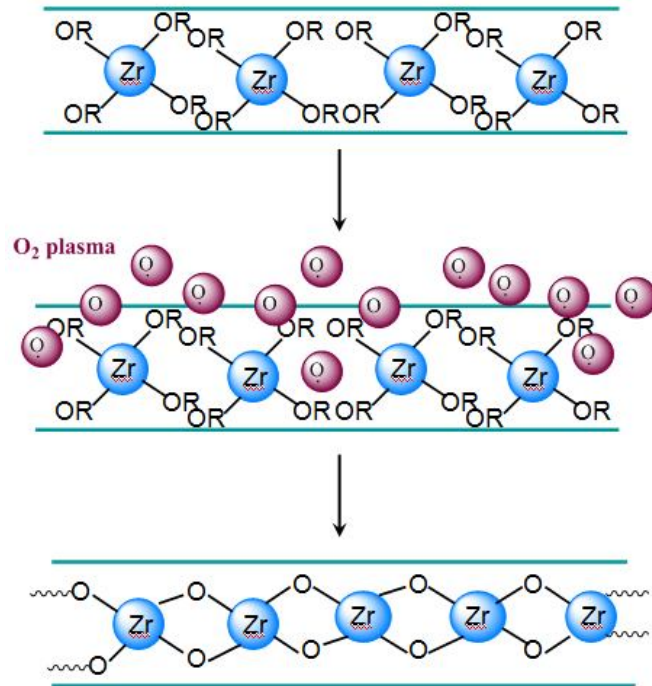


Figure 2-8 Mechanism of Zr-based sol-gel solution treated with oxygen plasma


2.7 Non-ideal phenomena of ISFET: Optical effect, Hysteresis, Drift and Lifetime

The electrochemical-sensing device generally has two primary non-ideal characteristics: the outer non-ideal characteristic (optical effect) and the inner non-ideal characteristics (drift effect and hysteretic effect). The total response of pH-ISFET consists of three parts: fast response, slow response and drift. The response of an ISFET to a fast pH step is general characterized by a fast response, followed by a slow change in the same direction, i.e. slow response, and ultimately a drift which is linear or logarithmic with time [18]. The fast response time is defined to be the time needed for the output to change from 10% to 90% of the total variation (at the order of ms or faster). The slow response is the extra time needed for the response to reach 100% . The drift is defined as the monotonic change of response after a proper time from the response (ex. 5 hours).

2.7.1. Optical effect

Because the measurement environment contains light exposure, we must consider the optical effect upon the sensing thin films or devices. Voorthuyzen and Bergveld [19] were the first to investigate the slow response of the Ta_2O_5 gate ISFET after illumination. Chiang et al. [20] reported on the light-induced characteristics of AlN pH-ISFET devices in the I–V measurement system. Their experimental results show that the output voltages changed when the light was switched on and off. The variation in the output voltage about was 16.8 mV.

2.7.2 Hysteresis



The amplitude of the slow response is quite small (3% to 7% of the total pH response) but will last for several hours [21]. This is because the slow response is correlated to the response of reactive sites in the bulk, i.e. buried sites, of the film, not like the fast response is related to the surface reaction [22],[23]. Because the ions have to diffuse to the buried sites for reaction, it will take a long time for response. The slow response will make small part of the pH response slowly, and occurs with a delay of the order of minutes to hours after the pH variation. There will have different output voltage, when the pH-ISFET was measured many times at the same pH value [24], and we call this phenomena is ” Hysteresis” or ”Memory effect”, still memory the original pH state.

2.7.3 Drift

When the intrinsic response (fast and slow response) is completed, the output

voltage of the pH-ISFET still varies with time gradually and monotonically. This phenomenon is called "Drift". According to Ref [18], it is difficult to identify the cause of this phenomenon, which could be either a surface or a bulk effect, or both. Some possible causes of drift have been proposed [18]. In 1998, Jamasb proposed a physical model quantitatively explains drift in terms of hydration of the silicon nitride surface [25]. This is the first physical model that provides a quantitative description of the drift characteristics.

He proposed that the surface of a silicon nitride film is known to undergo a relatively slow conversion to a hydrated SiO_2 layer or an oxynitride during contact with an aqueous solution. Since hydration alters the chemical composition of the nitride surface, then the dielectric constant of the overall insulator capacitor, i.e. the series combination capacitor of the superficial hydrated layer and that of the underlying silicon nitride, will exhibit a slow, temporal change. Consequently, the amount of the inversion charge stored in the semiconductor at a given gate bias slowly changes over time, giving rise to a monotonic temporal change in the threshold voltage [25]. The new idea sounds make sense for explaining drift mechanism. The author uses a new diffusion concept, dispersive transport, to model the transport mechanism.

Dispersive transport is proposed by Scher and Montroll in 1975 for explaining the phenomenon of the long tail photocurrent $I(t)$ in photoconductor like As_2Se_3 , which can not be explained by traditional Gaussian diffusion theory [26] [27]. They use an stochastic transport model based on time-dependent continuous-time random walk to interpret dispersive transport. Dispersive transport does not depend on the details of any specific mechanisms, but characterizes the motion of a carrier subjected to a broad distribution of event times. The event times include (1) hopping times from hopping transport (2) trap release times from multiple-trap transport (3) or both (1) and (2) that is

from trap-controlled hopping transport. In ISFET, sites may be the buried sites beneath the sensing layer surface and traps may be the dangling bond in the sensing films.

The carriers transport in an amorphous insulating material, which considered as a network of localized sites, by a succession of hops from one site to another. Because the distance between various neighboring sites have some variation than a mean value, the effective intersite transition rates

$$W(r) = W_0 e^{-r/r_0} e^{-\Delta/kT} \quad (2-18)$$

where r is the difference in position, Δ is the energy level of the sites, r_0 is the radius of the local charge distribution. We can know that $W(r)$ is sensitive to the sites distance, and will suffer a wide statistical dispersion. This is turning yields a broad distribution of hopping times [26] [27]. The authors designate a hopping time distribution function $\psi(t)$ to describe the time distribution, the probability per unit time for a carrier to hop at a time t , at any sites when the previous hop occurred at $t=0$. $\int_0^t \psi(t)dt$ will be the probability that after a carrier arrives in a given cell.

And by Ref [28], Dispersive transport is characterized by a power-law time decay of the mobility or diffusivity of the form $t^{\beta-1}$, $0 < \beta < 1$. Dispersive transport leads to a decay in the density of site/traps occupied by the species undergoing transport and the hydrated layer is essentially limited by dispersive transport in the presence of these sites/traps. The thickness of this hydrated layer will exhibit stretched-exponential time dependence. That is

$$\Delta N_{S/T}(t) = \Delta N_{S/T}(0) \exp\left[-(t/\tau)^\beta\right] \quad (2-19)$$

where $\Delta N_{S/T}(t)$ is the area density (units of cm^{-2}) of sites/traps occupied, τ is the time constant associated with structural relaxation, and β is the dispersion parameter characterizing dispersive transport.

2.8 References

- [1] S. Jamasb, S. D. Collins, R. L. Smith, A physical model for threshold voltage instability in Si₃N₄-gate H⁺-sensitive FET's (pH ISFET's), IEEE Transactions on Electron Devices 45 (1998) 1239-1245.
- [2] Y. Q. Miao, J. R. Chen, K. M. Fang, New technology for the detection of pH, Journal of Biochemical and Biophysical methods 63 (2005) 1-9.
- [3] S. Sfrenson, Enzyme studies II: the measurement and meaning of hydrogen ion concentration in enzymatic processes, Biochemische Zeitschrift 21 (1909)131–200.
- [4] D. A. Skoog, D. M. West, F. J. Holler, Fundamentals of Analytical Chemistry, 7th ed., Philadelphia, PA: Saunders College Publishing, (1996).
- [5] T. Matsuo, M. Esashi, Methods of ISFET fabrication, Sensors and Actuators B 1 (1981) 77-96.
- [6] M. Grattarola, G. Massobrio, Bioelectronics handbook: MOSFETs, biosensors, and neurons, McGraw-Hill, New York, (1998).
- [7] P. Bergveld, Thirty years of ISFETOLOGY What happened in the past 30 years and what may happen in the next 30 years, Sensors and Actuators B 88 (2003)1-20
- [8] W. Olthuis, Chemical and physical FET-based sensors or variations on an equation, Sensors and Actuators B 105 (2005) 96-103.
- [9] D. E. Yates, S. Levine, T. W. Healy, Site-binding model of the electrical double layer at the oxide/water interface, Journal of the Chemical Society-Faraday Transactions 70 (1974) 1807-1818.
- [10] L. Bousse, N. F. de Rooij, P. Bergveld, Operation of chemically sensitive field-effect sensors as a function of the insulator-electrolyte interface, IEEE Transactions on Electron Devices 30 (1983) 1263-1270.
- [11] R. E. G. van Hal, J. C. T. Eijkel, P. Bergveld, A novel description of ISFET

sensitivity with the buffer capacity and double-layer capacitor as key parameters, *Sensors and Actuators B* 24 (1995) 201-205.

[12] R. E. G. van Hal, J. C. T. Eijkel, P. Bergveld, A general model to describe the electrostatic potential at electrolyte oxide interfaces, *Advances in Colloid and Interface Science* 69 (1996) 31-62.

[13] C. D. Fung, P. W. Cheung, W. H. Ko, A generalized theory of an electrolyte-insulator-semiconductor FET, *IEEE Transactions on Electron Devices* 33 (1986) 8-18.

[14] D. L. Harame, L. J. Bousse, J. D. Shott, J. D. Meindl, Ion-sensing devices with silicon nitride and borosilicate glass insulator, *IEEE Transactions on Electron Devices* 34 (1987) 1700-1707.

[15] Dr. Ir. P. Bergveld Em University of Twente, ISFET, Theory and Practice, IEEE sensor conference Toronto (2003) 1-26.

[16] C. J. Brinker, G. W. Scherer, *Sol-Gel Science: The Physics and Chemistry of Sol-Gel Processing*, Academic Press (1990).

[17] L. L. Hench, J. K. West, The Sol-Gel Process, *Chemical Reviews* 90 (1990) 33.

[18] L. Bousse, P. Bergveld, The Role Of Buried OH Sites In The Response Mechanism Of Inorganic-Gate pH-Sensitive ISFETs, *Sensors and Actuators* 6 (1984) 65-78,.

[19] J. A. Voorthuyzen, P. Bergveld, Photoelectric effects in Ta₂O₅-SiO₂-Si structures, *Sensors Actuators B* 1 (1990) 350-353.

[20] J. L. Chiang, J. C. Chou, Y. C. Chen, Study on light and temperature properties of AlN pH-ion-sensitive-field-effect transistor devices, *Japanese Journal of Applied Physics* 44 (2005) 4831-4837.

[21] P. Woias, L. Meixner, P. Frostl, Slow pH response effects of silicon nitride ISFET sensors, *Sensors and Actuators B* 48 (1998) 501-504.

[22] J. C. Chou, K. Y. Huang, J. S. Lin, Simulation of time-dependent effects of

pH-ISFETs, Sensors and Actuators B 62 (2000) 88-91.

[23] L. Bousse, Comparison of the hysteresis of Ta₂O₅ and Si₃N₄ pH-sensing insulators, Sensors and Actuators B 17 (1994) 157-164.

[24] J. C. Chou, Y. F. Wang, Preparation and study on the drift and hysteresis properties of the tin oxide gate ISFET by the sol-gel method, Sensors and Actuators B 86 (2002) 58-62.

[25] S. Jamasb, S. D. Collins, R. L. Smith, A Physical Model for Threshold Voltage Instability in Si₃N₄-Gate H⁺-Sensitive FET'S (pH ISFET's), IEEE Transactions on Electron Devices 45 (1998) 1239-1245.

[26] H. Scher, E. W. Montroll, Anomalous transit-time dispersion in amorphous solid, Physical Review B 12 (1975) 2455-2477.

[27] G. Pfister, H. Scher, Time-dependent electrical transport in amorphous solid: As₂Se₃, Physical Review B 15 (1977) 2062-2082.

[28] J. Kakalios, R. A. Street, W. B. Jackson, Stretched-Exponential Relaxation Arising from Dispersive Diffusion of Hydrogen in Amorphous Silicon, Physical Review Letters 59 (1987) 1037-1040.

Chapter 3

Experiment and Measurement

3.1 Introduction

The difference between MOSFET and ISFET procedure is the process of gate electrode. The EIS (electrolyte-insulator-semiconductor) structure of ISFET take the gate membrane as a sensing layer immersed in the pH-solution [1], and the reference electrode is placed overhead the sensing layer as the gate voltage controller. This chapter depicts how to make the ZrO₂ sensing layer by sol-gel process, and construct EIS structure for pH sensing. The next section is the fabrication process flow of the pH-Ion-sensitive capacitor devices which are used for investigating the drift and hysteresis characteristics. And then, the measurement setup, and the detection principles of pH, hysteresis and drift will be presented. Finally, we make the application of ZrO₂ EIS capacitor for urea biosensor.

3.1.1 Reagent

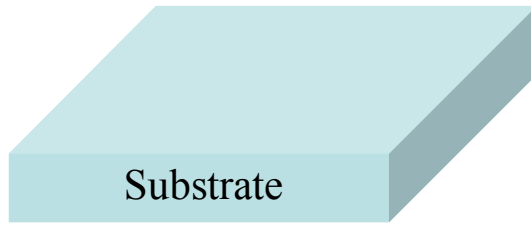
- (1) ZrCl₄, Zirconium(IV) chloride, Zirconium tetrachloride, assay : $\geq 99.9\%$ trace metals basis, manufacturer : Aldrich
- (2) IPA, 2-Propanol, assay : 99+%, manufacturer : Aldrich
- (3) Urea, molecular formula : CH₄N₂O, assay : $\geq 98\%$, manufacturer : Sigma
- (4) Urease, type III from Jack Beans, Enzyme Commission (EC) Number : 3.5 1.5, assay : 15,000-50,000 units/g solid, manufacturer : Sigma
- (5) Cellulose acetate, assay : 17 WT. % butyryl content, average MN CA. 65000,

manufacturer : Aldrich

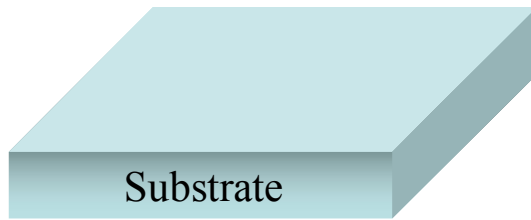
3.2 Fabrication Process

The fabrication process flow of this research is showed in Figure 3-1. The preceding procedures (from a. to e.) of experiment are done in NDL (National Nano Device Laboratory), similar to the manufacturing process of MOSFET [2]. Then the following section described thoroughly the sol-gel processes for ZrO_2 high- κ layers, and how to construct EIS capacitor structure. The fabrication parameters and procedures are listed as follows:

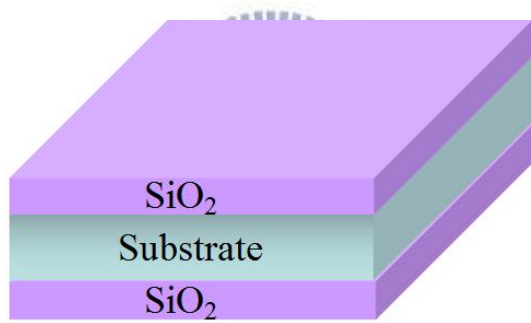
- a. Prepare prime Si wafer, RCA clean
- b. Proceed to Ion Implantation Processes
- c. Wet Oxidation Furnace for drive-in and annealing
- d. Standard clean for cleaning wafer surface and removing unnecessary SiO_2
- e. Wet-oxidation, 1000\AA
- f. TEL oxide etcher clear SiO_2 under the wafer
- g. The sol-gel process make high- κ ZrO_2 film on SiO_2
 - i. Prepare 0.017M ZrCl_4 solution in IPA
 - ii. Spin-coating the Zr-based solution on SiO_2
 - iii. Treating the sample by O_2 plasma for 5min
 - iv. Annealing 450°C for 1hr
- h. Photolithography for defining the sensing area
- i. Al electrode 3000\AA deposited by thermal coator
- j. Using Ag gel to contact with SPE
- k. Encapsulated with polyolefin



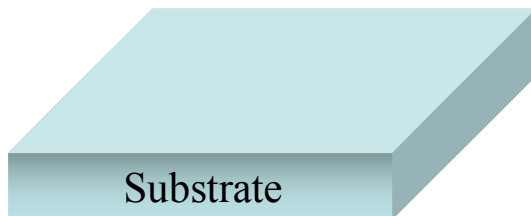
(a)



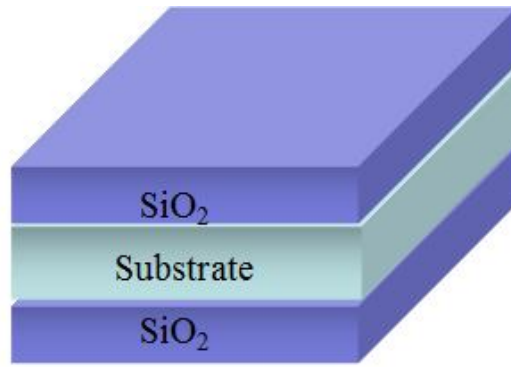
(b)



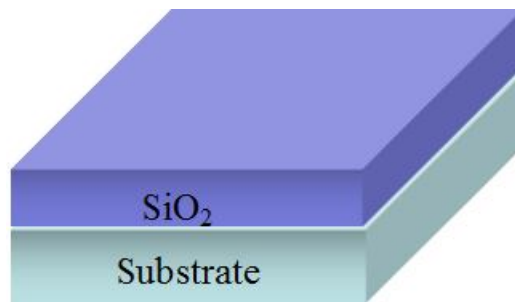
(c)



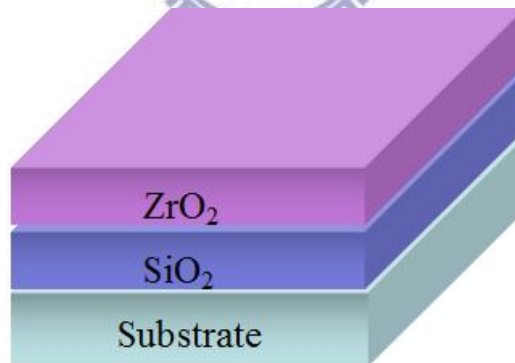
(d)



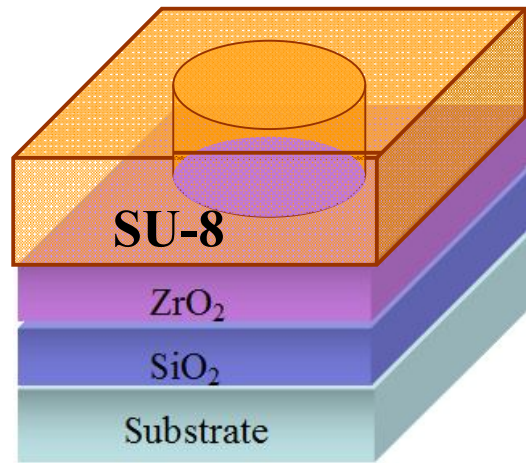
(e)



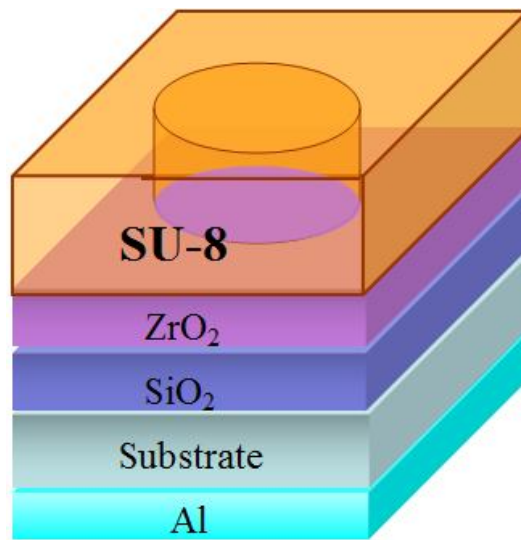
(f)



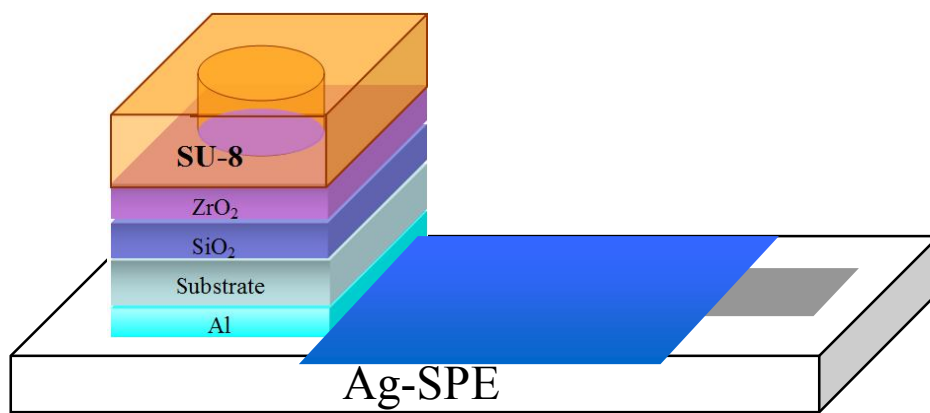
(g)



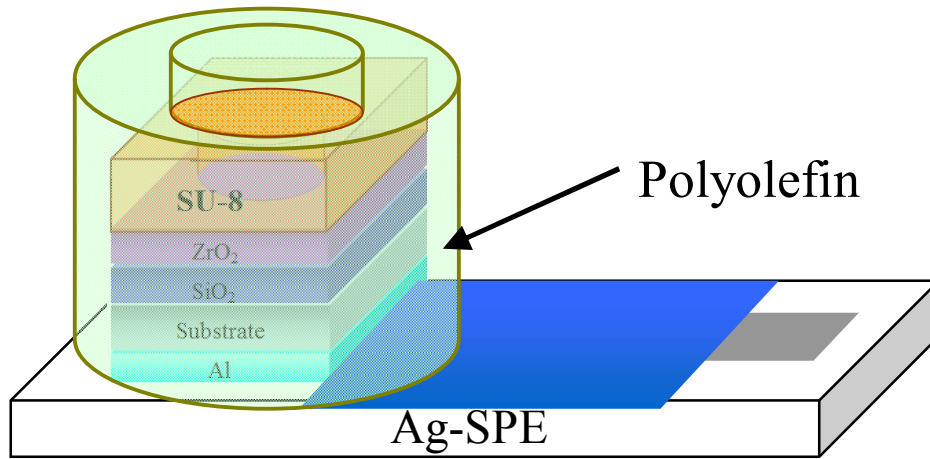
(h)



(i)



(j)



(k)

Figure 3-1 Fabrication process flow

3.3 The key steps of the experiment

3.3.1 Sensing layers fabrication



At first, we make a study of ZrO_2 high- κ layers by MIS structures as showed in Figure 3-2. Then we choose satisfied parameters to fabricate EIS capacitor.

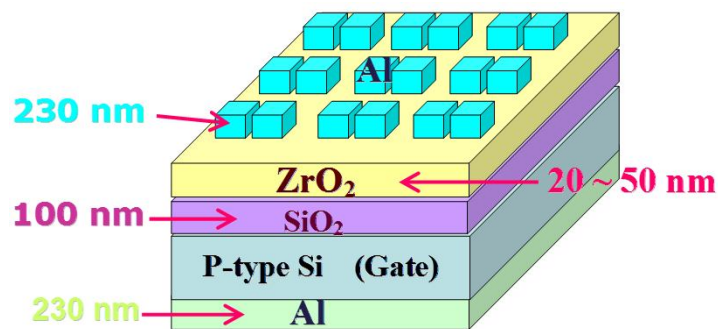


Figure 3-2 MIS structure with ZrO_2

This experiment of ZrO_2 sensing layers fabrication included many different parameters in the sol-gel processes. There are various control factors could impact the

characters of ZrO₂ sensing layers:

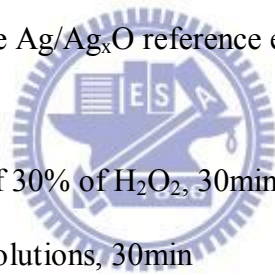
- a. The concentration of ZrCl₄ solution
- b. Times of spin-coating
- c. O₂ plasma treatment
- d. Annealing temperature
- e. Thickness of ZrO₂
- f. Photo Lithography

The results for foregoing impact factors were presented in next chapter.

3.3.2 Ag/Ag_xO reference electrode

Following steps are the solid-state Ag/Ag_xO reference electrode fabrication:

- a. Use the Ag-SPE
- b. Treated with few μ ls of 30% of H₂O₂, 30min
- c. Followed by 3M KCl solutions, 30min
- d. Rinse the electrodes with DI water
- e. Ag/Ag_xO reference electrodes is demonstrated



3.3.3 Photo Lithography

We tried to use photo-lithography to definite our sensing range and improve the quality of EIS capacitor. The process flow of photo-lithography is shown as follows:

- a. Bake at 180°C for 1 hr to dehydrate
- b. Coat HMDS on EIS capacitor with ZrO₂ sensing film
- c. Bake at 60°C for 1 hr to evaporate
- d. Coat SU-8 2005 (500 rpm for 5 s, then 3000 rpm for 30 s)

- e. Edge bead removal (EBR)
- f. Soft baking the SU-8 2005 to remove unnecessary solvent (65°C for 1 min, then 95°C for 2 min)
- g. Exposing the SU-8 to Hg lamp system (15 s in 38.6 mJ/cm²)
- h. Post exposure bake (65°C for 1 min, then 95°C for 2 min)
- i. Develop (immerse in SU-8 developer for 20~30 s in r.t.)
- j. Rinse and dry
- k. Hard bake (150°C for 30 min)

3.3.4 Urea biosensor

Entrapment method was used for immobilization of urease onto EIS capacitor with ZrO₂. In this case, 0.2 mL of 50 mg mL⁻¹ urease solution prepared in 0.1 mol L⁻¹ borate buffer pH 10 were deposited on the ZrO₂, which was kept at 4°C until complete solvent evaporation. Then, 0.2 mL of cellulose acetate 1% w/w in acetone was added onto the electrode. It was again kept at 4°C and after complete solvent evaporation the amperometric tests were performed.

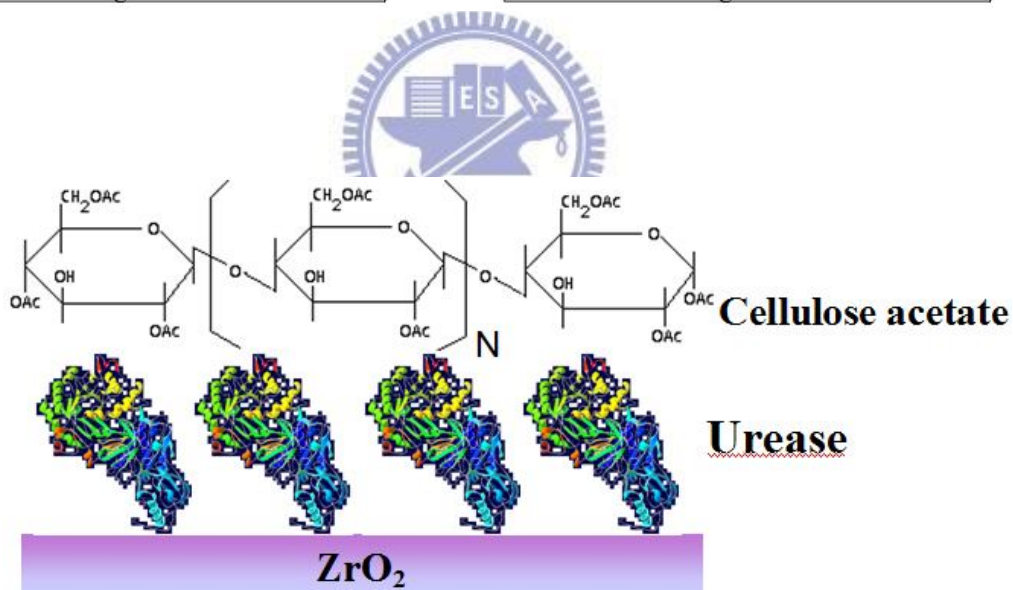
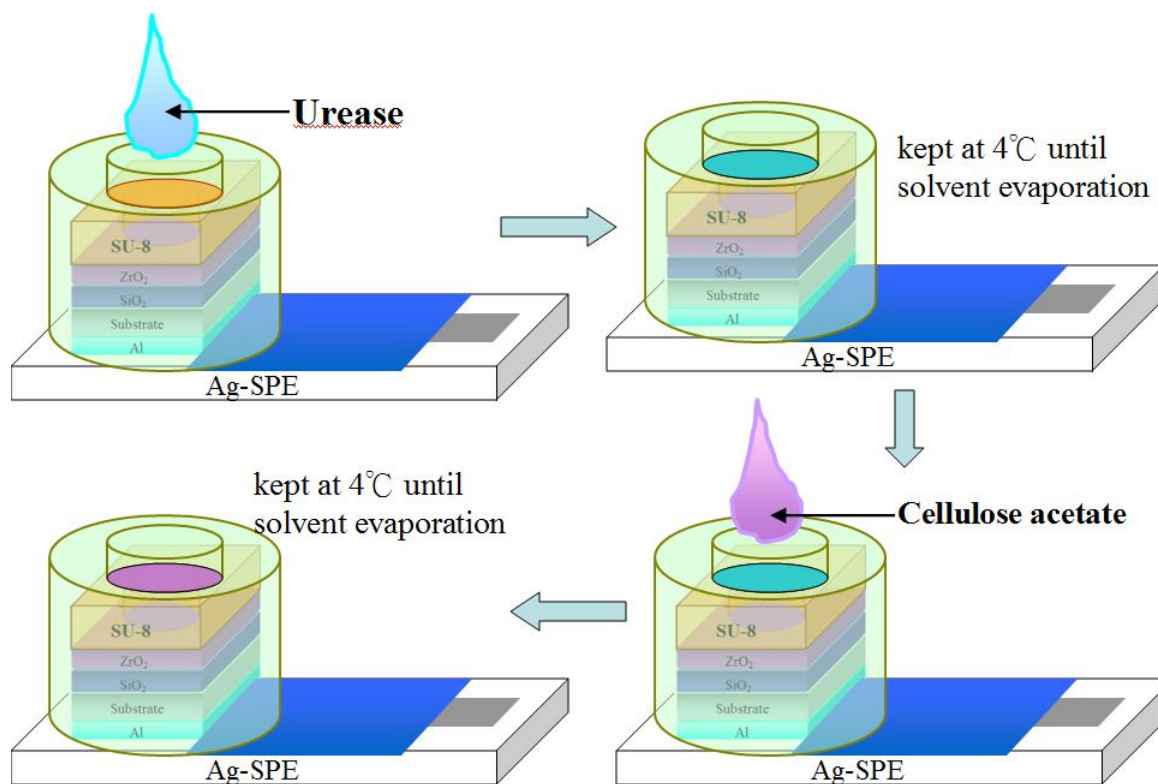


Figure 3-3 Fabrication process flow of urease immobilization

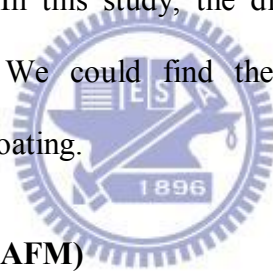
The enzyme immobilization method is entrapment in physical barrier of cellulose acetate. The immobilization method consisted of the entrapment of this bimolecular inside a cellulose acetate polymeric network, aiming, for example, to reduce loss by leaching of the enzyme, one of the major problems found in this area of research. One

advantage of this method is that conformational changes in the enzyme structure seldom happen, preserving its biological activity [3, 4].

3.4 Analyze structural properties

3.4.1 Scanning electron microscope (SEM)

The SEM is a type of electron microscope that images the sample surface by scanning it with a high-energy beam of electrons in a raster scan pattern. The electrons interact with the atoms that make up the sample producing signals that contain information about the sample's surface topography, composition and other properties such as electrical conductivity. In this study, the different thickness of ZrO₂ sensing layers was assayed by SEM. We could find the relationship between thickness, concentration and times of spin-coating.



3.4.2 Atomic force microscopy (AFM)

The AFM consists of a cantilever with a sharp tip (probe) at its end that is used to scan the specimen surface. When the tip is brought into proximity of a sample surface, forces between the tip and the sample lead to a deflection of the cantilever according to Hooke's law. AFM is a very high-resolution type of scanning probe microscopy, with demonstrated resolution of fractions of a nanometer. AFM was used to analyze surface roughness of ZrO₂ at different annealing temperature for this research.

3.4.3 X-ray crystallography (XRD)

XRD is a method of determining the arrangement of atoms within a crystal, in which

a beam of X-rays strikes a crystal and diffracts into many specific directions. From the angles and intensities of these diffracted beams, a crystallographer can produce a three-dimensional picture of the density of electrons within the crystal. From this electron density, the mean positions of the atoms in the crystal can be determined, as well as their chemical bonds, their disorder and various other information. The analysis of XRD can indicate crystals of ZrO_2 at different annealing temperature.

3.5 Measurement system

3.5.1 Preparation of measurement

We measured the C-V curves for the pH-Ion-sensitive capacitor by using as measurement tool and the system to investigate the characteristics of the ZrO_2 as sensing layers. For getting correct result of measurement, the entire measurement procedures were executed in a dark box to prevent light influence and the electromagnetic wave.

There are two package methods for EIS capacitor, microfluidic channel and extended-gate-field-effect-transistor (EGFET). We had tried both of them and choose the suitable method—EGFET. In order to make the EIS capacitor and reference electrode immersed in the aqueous solution, we use Ag-SPEs (Zensor Inc.) act as subtracts to extend gate and connect with alligator clips.

The pH-standard solution is purchased by Merck & Co. Inc., and the pH-values are 2, 4, 6, 8, 10 and 12. The electric potential of the pH-solution will be floating [6] during open-loop circuit. The disturbance from the environment would induce the electric potential variance of the solution. By eliminating this variance, a reference electrode is needed to immersion in the pH-solution to close the circuit loop.

3.5.2 Capacitance -Voltage measurement set-up

A KEITHLEY-590、595 semiconductor parameter analyzer system were set up to measure the capacitance-voltage (C-V) characteristics curves and the system is shown in Fig. 3-3.. All measurements were arranged in a dark box to minimize the effects of photoelectric and temperature. In the setup of KEITHLEY-590、595, substrate voltage is ground to avoid the body effect and the reference electrode is sweeping to different voltage. In the measurement of sensitivity, the response of the EIS capacitor is the function of time. According to P. Woias [5], the first equilibrium will achieves in a minute.

We set the frequency for 1MHz in capacitance-voltage analyzer system. In order to obtain the sensitivity, at first we measure the C-V to observed the flat-band condition and depletion region. Secondly, we make the subtract voltage (V_{sub}) sweep the range to measure C-V from pH 2 to pH 12 in turn. As changing the pH buffer solution, we diluted next butter solution which under test twice, and stay 1 min to avoid the effect of the buffer solution that measured before. The variation of the subtract voltage exhibits the pH sensitivity of the sensing oxide.

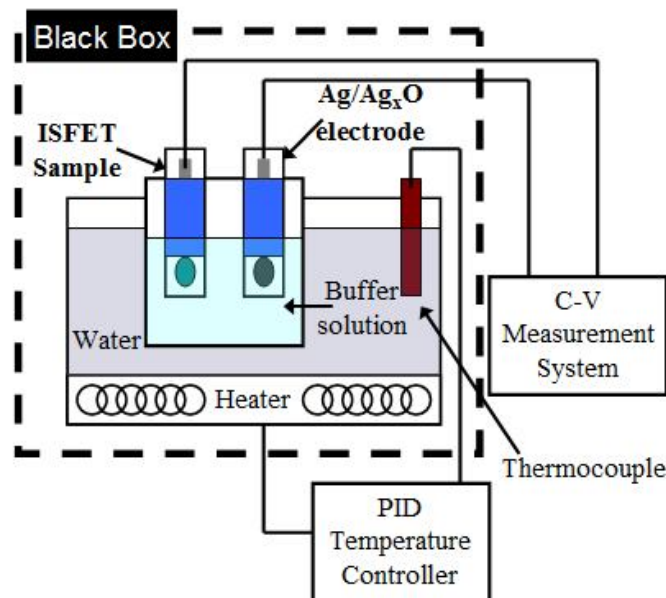


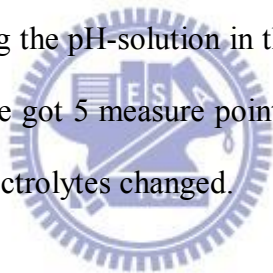
Figure 3-4 Schematic of the C-V measurement system.

3.5.3 Drift measurement set-up

The drift characteristics were measured with pH = 7 of aqueous buffer solution and the same condition samples period of 1 minute, 5 minutes and 10 minutes. 88 sampling points in the time frame of 8 hours and 40 mins were observed for EIS capacitor with ZrO₂. The detection principle is in a similar manner to that of the pH measurement.

3.5.4 Hysteresis measurement set-up

For characterizing the hysteresis phenomena of EIS capacitors, we measured C-V curves for etch film with changing the pH-solution in the order of pH 7-4-7-10-7, and pH 7-10-7-4-7. For each pH value we got 5 measure points with duration of 5 min, detailed dilute works were done before electrolytes changed.



3.5.5 Urea biosensor measurement set-up

In the study of urea biosensor, at first, we investigated the enzyme working spacer of urease. Then we measured C-V curves of ZrO₂ EIS capacitor thoroughly in the pH range, and the pH-values are 4.8, 5.4, 6, 6.6, 7.2, 7.8 and 8.4. Second, we prepared various concentration of urea solution (in pH 7 buffer solution), and make blank experiment to measure C-V curves of ZrO₂ EIS capacitor in urea solutions. The concentration of urea solutions are 3 mM, 10 mM, 20 mM, 30 mM and 40 mM.

Finally, we use EIS capacitor which immobilized urease to measure C-V curves in different concentration of urea solution. As a result, we could observe and compare the sensitivity for urea biosensors.

3.6 References

- [1] P. Bergveld, Thirty years of ISFETOLOGY What happened in the past 30 years and what may happen in the next 30 years, *Sensors and Actuators B* 88 (2003)1-20.
- [2] T. Matsuo, M. Esashi, Methods of ISFET fabrication, *Sensors and Actuator B* 1 (1981) 77-96.
- [3] B. Lakard, G. Herlem, S. Lakard, A. Antoniou, B. Fahys, Urea potentiometric biosensor based on modified electrodes with urease immobilized on polyethylenimine films, *Biosensors and Bioelectronics* 19 (2004) 1641–1647.
- [4] M. Singh, N. Verma, A. K. Garg, N. Redhu, Urea biosensors, *Sensors and Actuators B* 134 (2008) 345–351.
- [5] P. Woias, L. Meixner, P. Frostl, Slow pH response effects of silicon nitride ISFET sensors, *Sensors and Actuator B* 48 (1998) 501.



Chapter 4

Results and Discussions

4.1 Introduction

In this chapter, we will discuss the results of sol-gel deposited ZrO_2 sensing layer for EIS capacitor. At first, we analyzed structural properties by SEM, AFM and XRD as shown in next section. Then we proved high- κ properties by MIS capacitors with ZrO_2 , and chose suitable parameters to make EIS capacitor. In the fabrication of EIS capacitor, the steps were simplified and solid-state reference electrode (Ag/Ag_xO reference electrode) was used. Finally, we discussed non-ideal phenomena (hysteresis and drift) in later section.



4.2 Structural properties

4.2.1 Scanning electron microscope (SEM)

In this study of SEM, we find the main factor of ZrO_2 thickness is the concentration of $ZrCl_4$ solution and the number of spin-coating layers. We chose the ZrO_2 films spin coated on SiO_2 surface for one layer and three layers, then, which were treated with O_2 plasma and annealing at $350^\circ C$ for 1 hr. The thickness of ZrO_2 films depended on concentration and the layer of spin-coating as shown in figure 4-1. The concentration of $ZrCl_4$ was 0.015 g/ml in ethanol. Figure 4-1 shows spin-coating one layer of ZrO_2 , and the thickness was 45 nm. From Dr. Hsin-Chiang You's study, the linear observation suggests that the film thickness is controllable and tunable by the Zr /hexanol ratio. They

can control the thickness of ZrO_2 films by change the concentration of ZrCl_4 precursor [1]. We also found the relationship between thickness and concentration and even observed the thickness of ZrO_2 can be connected with the times of spin-coating.

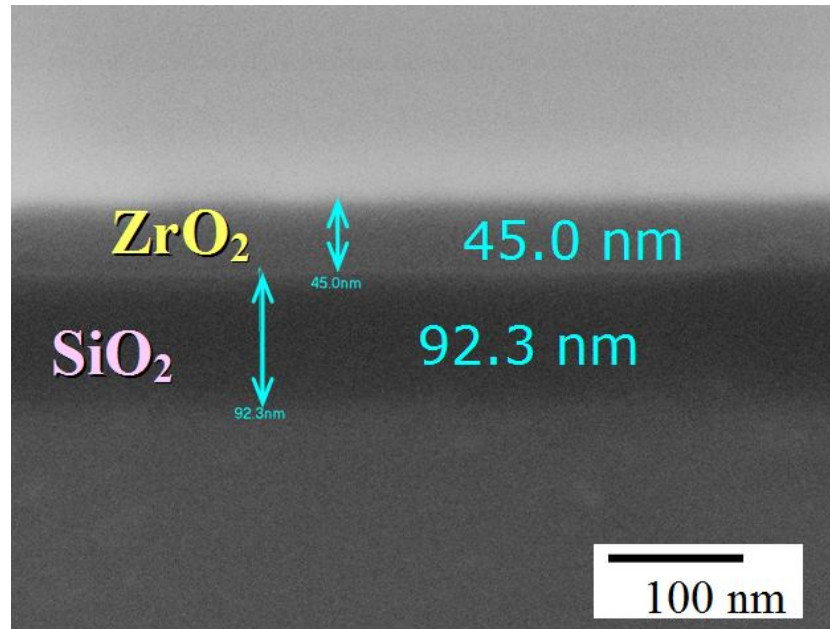


Figure 4-1 SEM image of one layer spin-coated ZrO_2 layer

4.2.2 Atomic force microscopy (AFM)

We used AFM to examine the surface morphologies and surface roughness of the $\text{ZrO}_2/\text{SiO}_2$ stacked films grown on the Si samples and then annealed at 350°C and 450°C , respectively. The surfaces of ZrO_2 films were smooth and the grain-size distributions in the films annealed at the higher temperatures were wider than those in the films annealed at lower temperatures, presumably because of the nucleation and growth of the films from the ZrO_2 . We attribute this behavior to the grain growth arising from the mobility to the constituents of the film during the annealing process [2]. The mean roughness of ZrO_2 film which was annealed at 350°C was 1.637 nm, and the mean roughness of ZrO_2 film which was annealed at 450°C was 1.635 nm as shown in figure 4-2 and 4-3, respectively.

Besides, it is generally accepted that during high-temperature annealing process, the oxygen atoms removed from the film mostly migrate to the surface and therefore leads to the formation of a layer of amorphous silica.

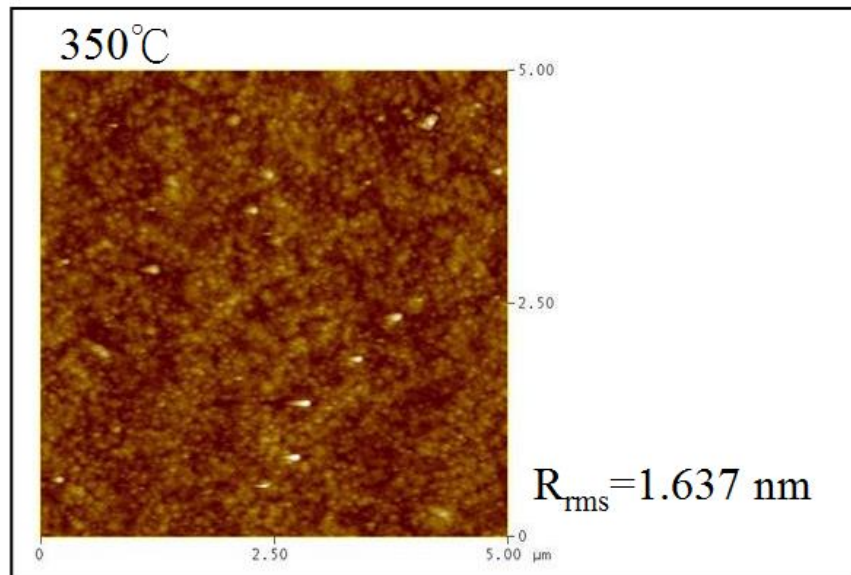


Figure 4-2 AFM image of ZrO_2 film surface (annealing at 350°C)

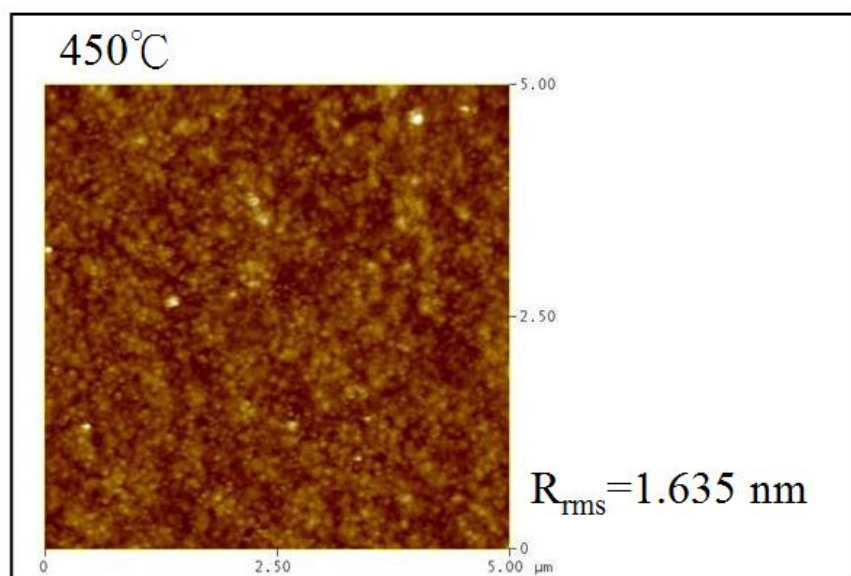


Figure 4-3 AFM image of ZrO_2 film surface (annealing at 450°C)

4.2.3 X-ray diffraction (XRD)

X-ray diffraction measurements were performed to study the effect of the annealing at varied temperatures (350°C and 450°C) on the crystalline nature of the ZrO₂ sensing layers. The sample which thermal annealed below 250°C showed no peak in XRD pattern, respectively, indicative of an amorphous structure. In the figure 4-4, with respect to the annealed sample at 350°C, two smaller m-ZrO₂ (0 1 1) and t-ZrO₂ (1 1 1) peaks were found at the 2θ degree, and a larger m-ZrO₂ (1 1 1) peak was found in the same pattern. The intensity of the m-ZrO₂ (1 1 1) reflection for the film annealed at 450°C is smaller than that of annealed at 350°C. This result suggests that the formation of a Zr-silicate layer at the ZrO₂/SiO₂ interface due to the diffusion of zirconium from the film to SiO₂. In the XRD pattern of the annealed sample at 450°C as shown in figure 4-5, t-ZrO₂ (1 1 1) peak was larger than m-ZrO₂ (1 1 1) peak. The XRD patterns of ZrO₂ referred to the unseeded and seeded samples annealed at different temperatures [3].

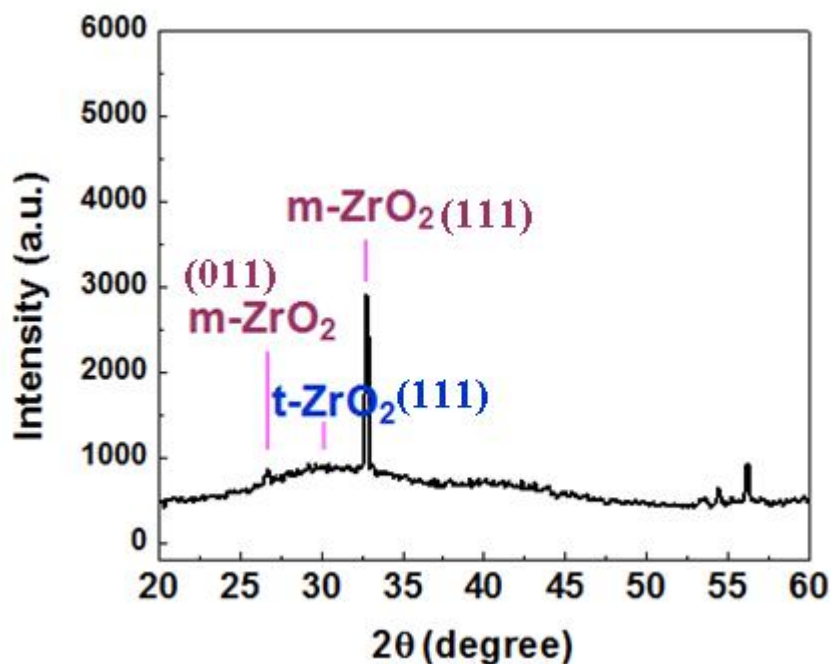


Figure 4-4 XRD pattern of ZrO₂ to EIS capacitor (annealing at 350°C)

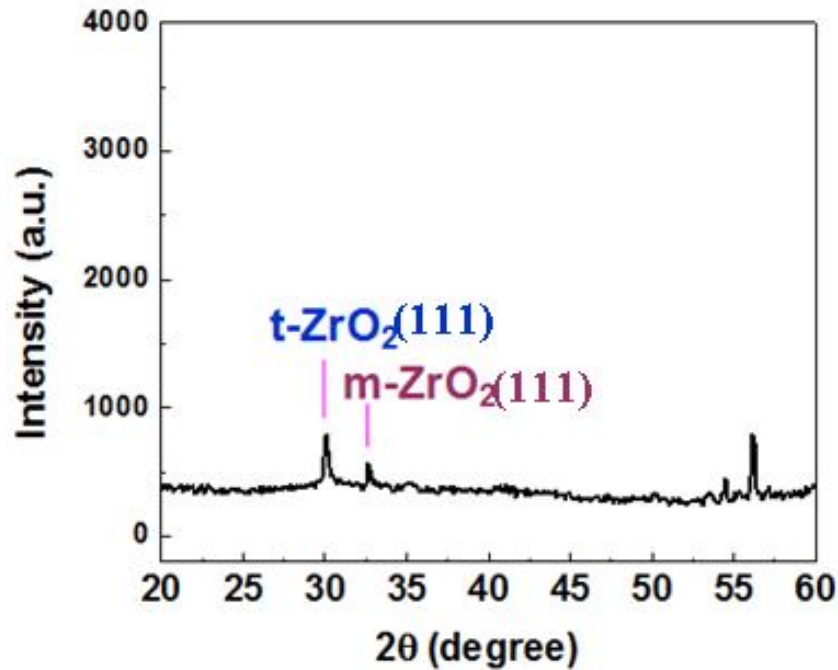


Figure 4-5 XRD pattern of ZrO₂ to EIS capacitor (annealing at 450°C)

4.2.4 Summary



According to the ref.1 and SEM image, the observation suggests that the ZrO₂ film thickness is controllable and tunable by the concentration of ZrCl₄ precursor and the times of spin-coating. Moreover, with respect to the influence of thermal annealing at varied temperatures on the surface nature of ZrO₂ sensing film, the out come of AFM analysis. It is obvious that the ZrO₂ film annealed at 350°C and 450°C exhibit smooth surface with root mean square roughness (*R*_{rms}) of 1.637 nm and 1.635 nm. Besides, to further investigate the influence of the O₂ plasma and annealing treatment on the compositional properties of the deposited ZrO₂ thin layer, XRD analysis was carried out. There are two different crystalline types (t-ZrO₂ and m-ZrO₂) of ZrO₂ thin layers which annealed at 350°C and 450°C. This result of XRD also proved that we could fabricate ZrO₂ crystalline membranes by sol-gel process included O₂ plasma and annealing treatment.

4.3 C-V curves of ZrO₂ to MIS capacitors

We fabricated MIS structure for testing the qualities and high- κ properties of ZrO₂ films. The C-V curves of ZrO₂ to MIS capacitor are in figure 4-6. From the capacitance density of different MIS capacitors, we could calculate the permittivity of SiO₂/ZrO₂ film by following formula :

$$C = \frac{\epsilon_0 \epsilon_{SiO_2/ZrO_2} A}{d}, \quad \epsilon_0 \approx 8.854 \times 10^{-12} \text{ Fm}^{-1}$$

In this result, the experimental permittivity of SiO₂ film was 3.16, and the experimental permittivity of SiO₂/ZrO₂ film was 4.75. The experimental dielectric constant of SiO₂ was 3.16 and ZrO₂ was 15. It manifested the high- κ properties of ZrO₂ film.

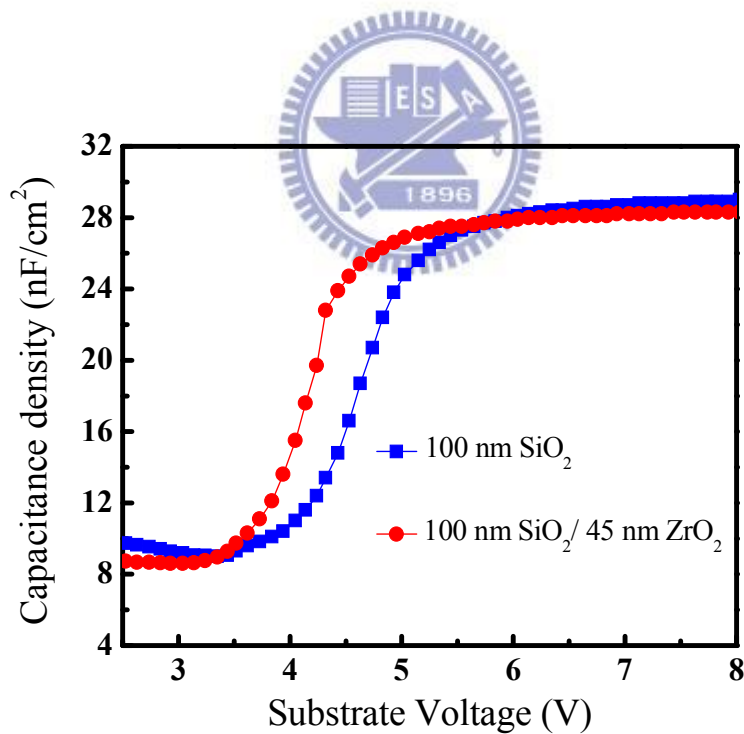


Figure 4-6 C-V curves of ZrO₂ to MIS capacitors

4.4 pH sensing performance of ZrO₂

In order to find suitable parameters to make EIS capacitor with ZrO₂, we chose some conditions to test the pH sensing performance of ZrO₂ as shown in figure 1-4. In pH-EIS sensing, the change of pH level normally leads to the flat-band voltage shift of the $C-V$ curves. This outcome is mainly due to the ionization of the surface hydroxyl groups by hydrogen ions or hydroxyl ions. In order to evaluate the sensing performance of the ZrO₂ membrane annealed at different temperatures, the $C-V$ curves of these cases studied at the pH levels ranging from pH 2 to pH 12 were experimentally investigated. It showed normalized $C-V$ curves of ZrO₂ to EIS capacitor without O₂ plasma in figure 4-7, and present bad $C-V$ curves in pH 2 and pH 4. We consider that O₂ plasma had really effect on fabricate ZrO₂ films, this effect was also found in MIS capacitor with ZrO₂.

Then we discussed the parameters of annealing temperature and spin-coating layers, and the normalized $C-V$ curves of ZrO₂ to EIS capacitor (annealing at 250°C) were in figure 4-8. The $C-V$ curves were not sharp and the capacitances were low in this sample. It is because of fixed oxide charge which can be decreased by higher temperature annealing. During higher temperature annealing, the silicon atom removed from the film mostly migrated to the interface and increased the formation of an amorphous silicate layer, resulting in a smaller surface roughness.

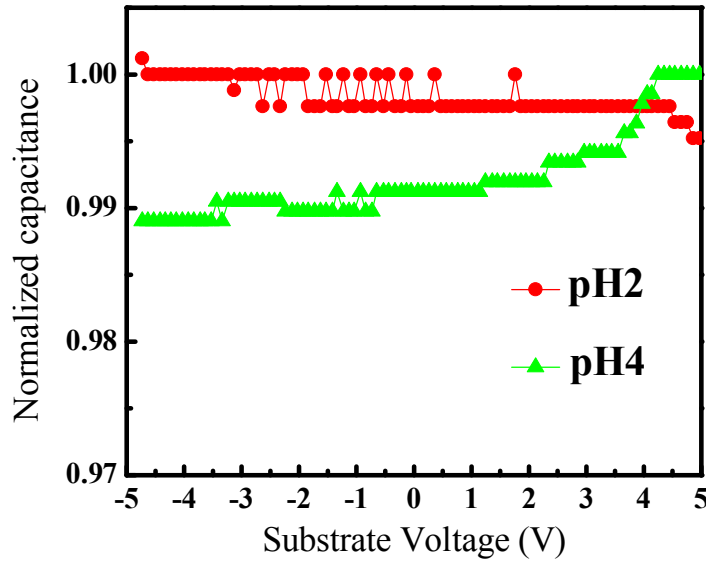


Figure 4-7 Normalized C-V curves of ZrO₂ to EIS capacitor without O₂ plasma

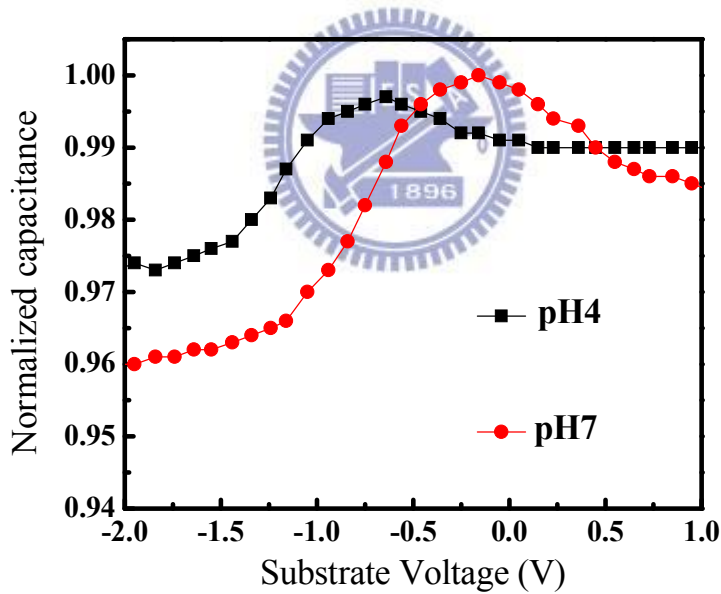
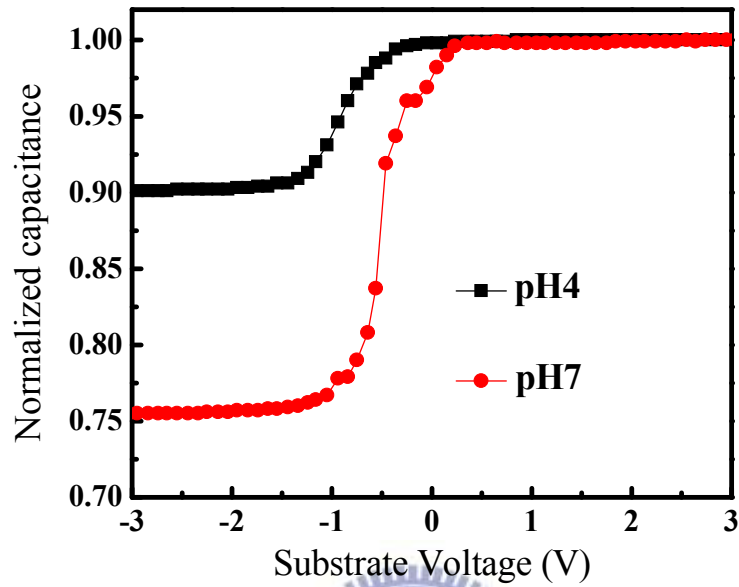


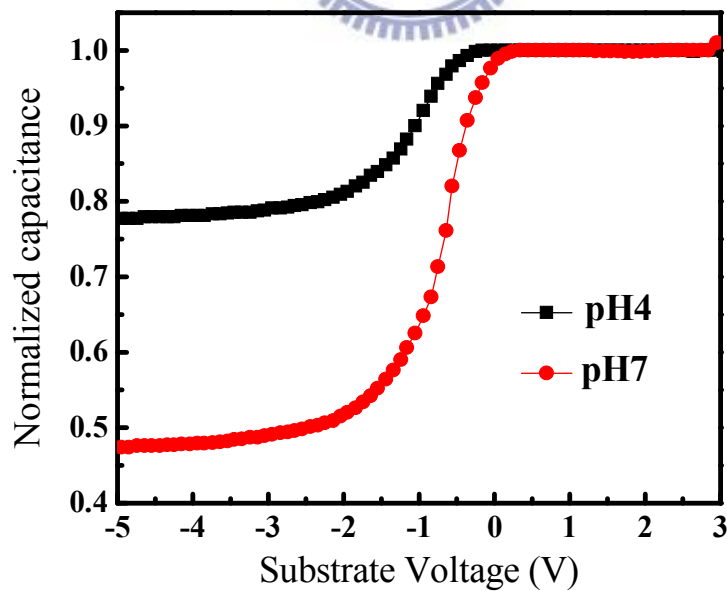
Figure 4-8 Normalized C-V curves of ZrO₂ to EIS capacitor (annealing at 250°C)

Figure 4-9, 4-10 are the normalized C-V curves of different kind EIS capacitor with ZrO₂. We observe that the sample with one layer of ZrO₂ film show sharper C-V curve and small depletion region than the sample with three layers of ZrO₂ films. There are some defects or traps in the interface between ZrO₂ films. So we chose annealing

temperature of 350, 450°C and one layer of ZrO₂ film to do further examination, the parameters are optimum.



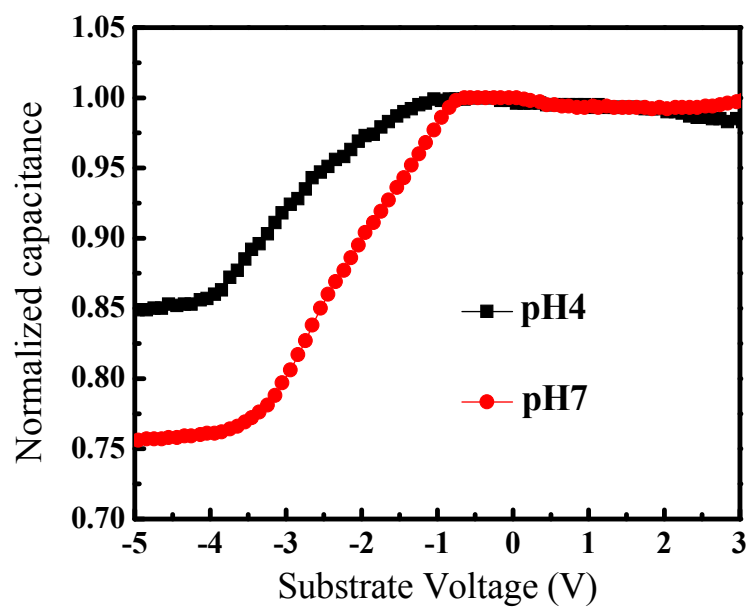
(a)



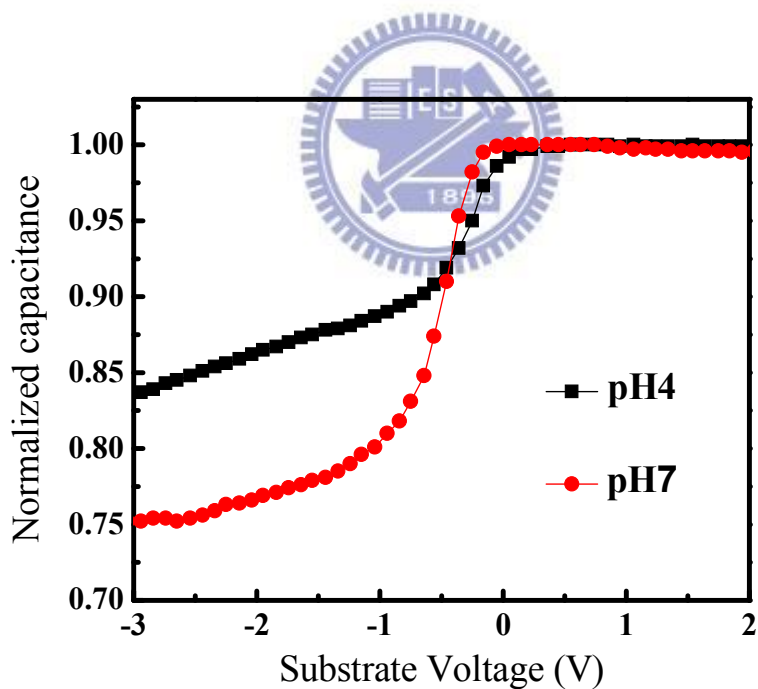
(b)

Figure 4-9 Normalized C-V curves of One layer ZrO₂ to EIS capacitor

(a)annealing at 350°C, (b) annealing at 450°C



(a)



(b)

Figure 4-10 Normalized C-V curves of three layers ZrO₂ to EIS capacitor

(a)annealing at 350°C, (b) annealing at 450°C

Figure 4-11, 4-12 show normalized C-V curves and sensitivity of ZrO₂ to EIS

capacitor (annealing at 350°C). It is found that EIS devices after annealed at 350°C show a high pH sensitivity of 59.32 mV/pH but low coefficient of correlation ($R=0.8936$). Figure 4-13, 4-14 are normalized C-V curves and sensitivity of ZrO_2 to EIS capacitor (annealing at 450°C). The EIS devices after annealed at 450°C show a lower pH sensitivity of 27.23 mV/pH and good coefficient of correlation ($R=0.9986$). It is well known fact that annealing treatments under oxygen ambient can improve the optical and structural properties of the metal oxides, due to the reduction of defect density and the optimization of oxide stoichiometry. The ZrO_2 sensing membrane of EIS device which was annealed in lower temperature must exist more defects and traps, so the sensing property would be unstable.

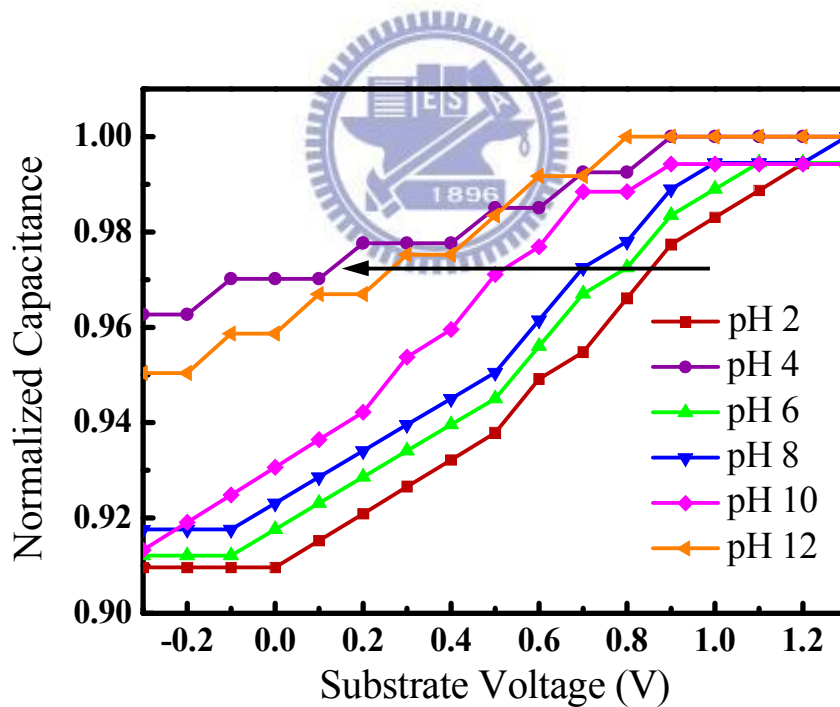


Figure 4-11 Normalized C-V curves of ZrO_2 to EIS capacitor (annealing at 350°C)

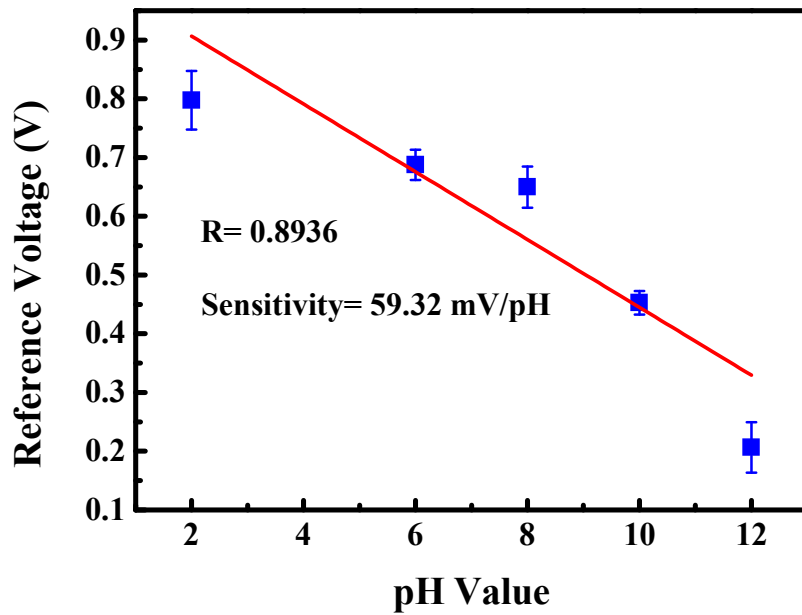


Figure 4-12 Sensitivity characteristic of ZrO_2 to EIS capacitor (annealing at 350°C)

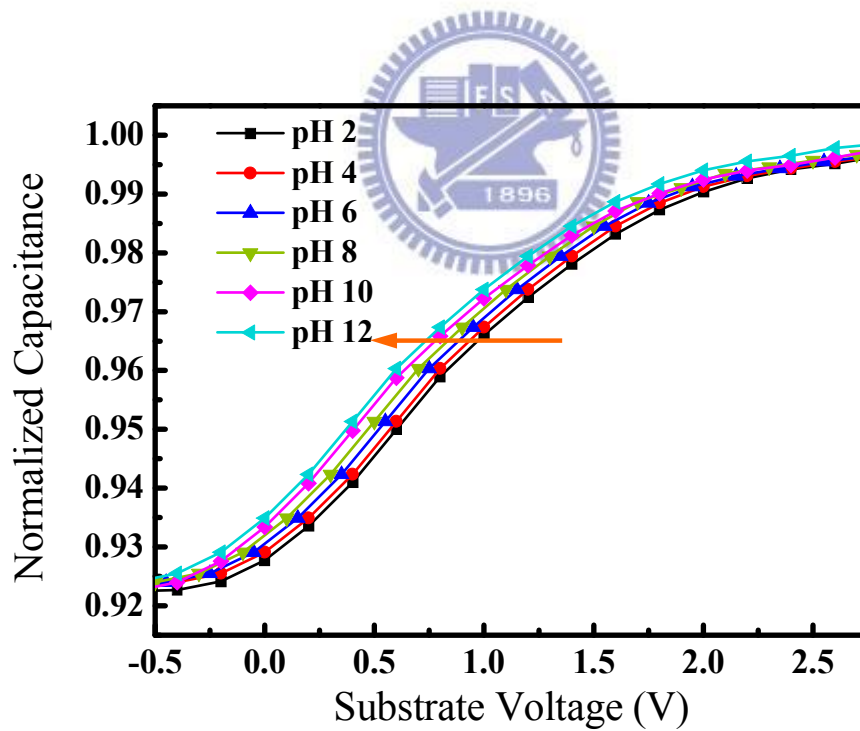


Figure 4-13 Normalized C-V curves of ZrO_2 to EIS capacitor (annealing at 450°C)

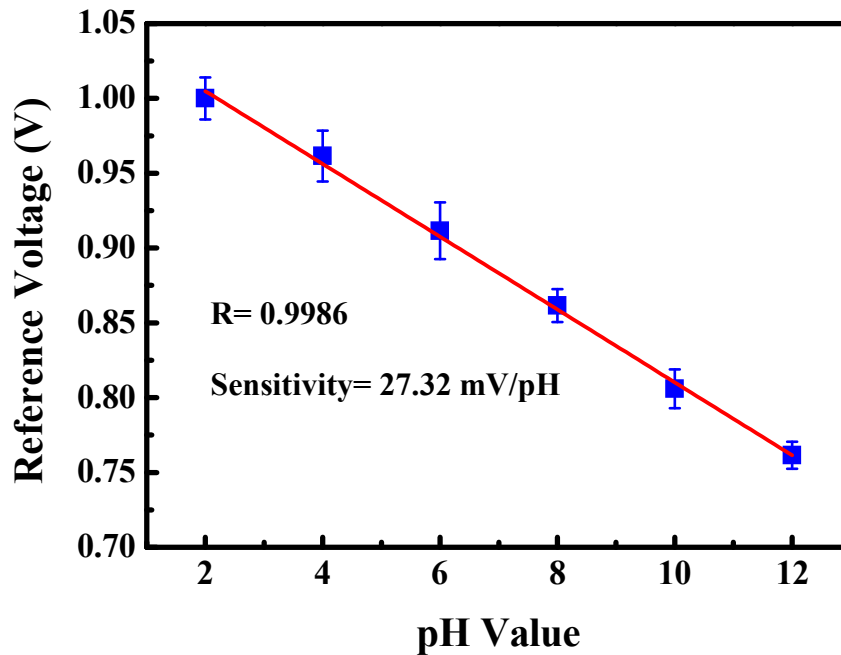


Figure 4-14 Sensitivity characteristic of ZrO_2 to EIS capacitor (annealing at $450^\circ C$)

These $C-V$ curves were shifted as a result of the surface potential modification by the change in the number of hydrogen ion on the sensing film. According to foregoing results, we observed the annealed sample at $450^\circ C$ show better linearity but lower pH sensitivity. The $C-V$ curves of annealed sample at $350^\circ C$ have lower and larger depletion region. And we also noted that the quality of annealed sample at $450^\circ C$ is better than the quality of annealed sample at $350^\circ C$ in the fabrication of EIS capacitor. The structure and sensitivity characteristics at different annealing temperature are shown in table 4-1. The annealed sample at $350^\circ C$ also has lower yield and reliability than the annealed sample at $450^\circ C$, and always exhibit extraordinary shift of $C-V$ curves in $pH \leq 4$ and $pH \geq 10$ buffer solution. The higher annealing temperature must make ZrO_2 film denser and increase the ability to resist acid or base.

	Mean Roughness	Major crystallization	R	Sensitivity
350°C	1.637 nm	m-ZrO ₂	-0.8936	59.32 mV/pH
450°C	1.635 nm	t-ZrO ₂	-0.9986	27.32 mV/pH

Table 4-1 The comparison of the structure and sensitivity characteristics at different annealing temperature

We also study the influence of photo-lithography in EIS capacitor fabrication. The sensing membrane size was defined through photolithographic processing under a photosensitive epoxy (SU8-2005, MicroChem Inc.) that behaves as an antiacid polymer. Figure 4-15, 16 are normalized C-V curves and sensitivity characteristic of ZrO₂ to EIS capacitor after photo-lithography (annealing at 450°C). And the diameter of sensing range is 2 mm. In this result, the annealed sample at 450°C after photo-lithography show higher pH sensitivity. It is found that EIS devices after annealed at 450°C and photo-lithography show a very high pH sensitivity of 94.13 mV/pH and good coefficient of correlation (R= 0.9536). We chose this parameter of ZrO₂ EIS capacitor to make following experiment of urea biosensor.

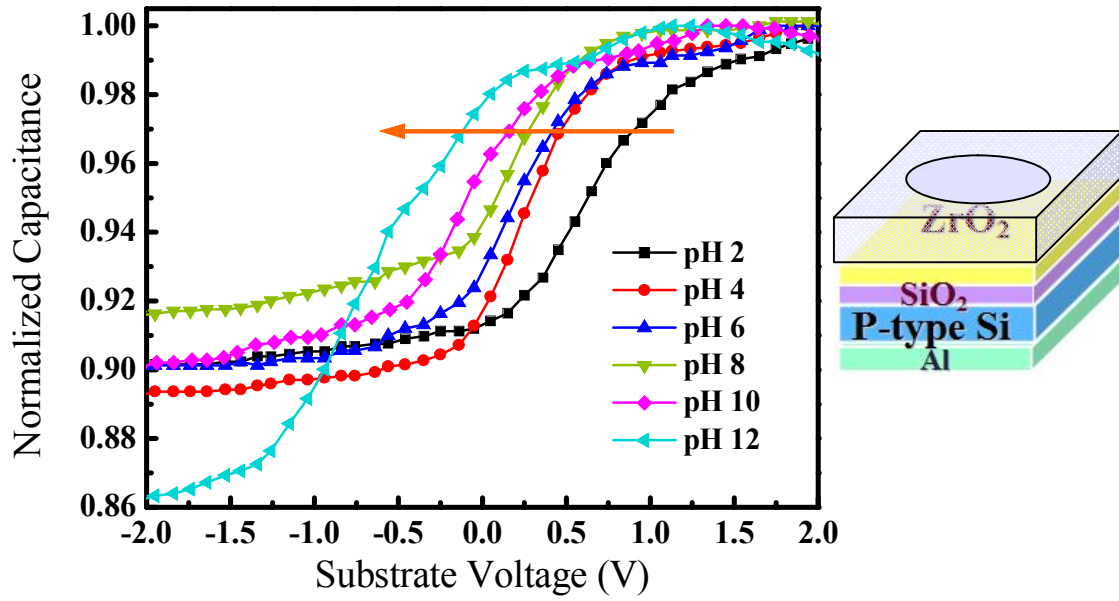


Figure 4-15 Normalized C-V curves of ZrO_2 to EIS capacitor after photo-lithography (annealing at $450^\circ C$)

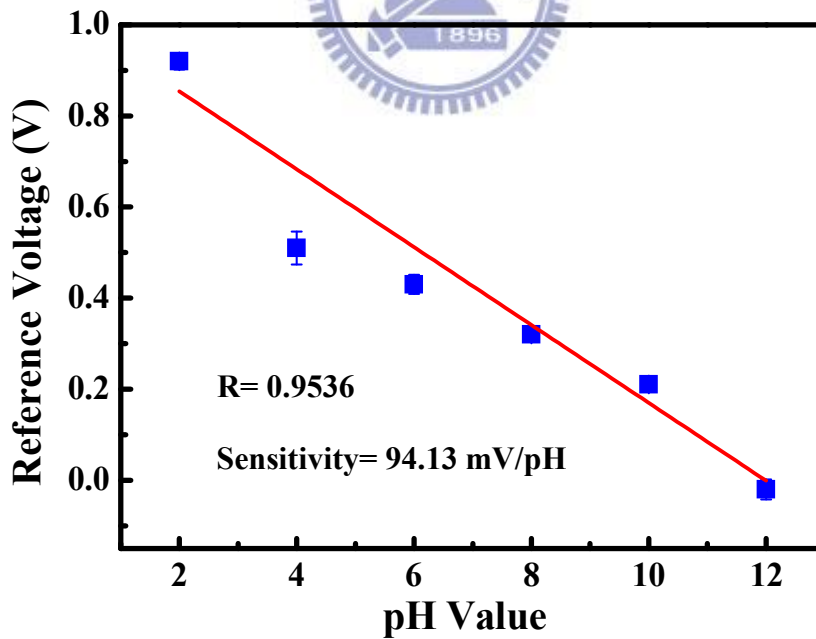


Figure 4-16 Sensitivity characteristic of ZrO_2 to EIS capacitor after photo-lithography (annealing at $450^\circ C$)

4.4.1 Summary

In sensing performance experiment of ZrO_2 EIS capacitor, we chose some control parameters such as O_2 plasma treatment, varied annealing temperature and times of spin-coating. At first, we observed that O_2 plasma treatment and higher annealing temperature are necessary for making ZrO_2 sensing membrane. Then the EIS capacitor with spin-coating one layer ZrO_2 has better property in $C-V$ curves than the EIS capacitor with three layers ZrO_2 . The quality and pH-sensing linearity of annealed device at 450°C is better, and the annealed device at 350°C has some problem for detection in $\text{pH} \leq 4$ and $\text{pH} \geq 10$. At last, the annealed device at 450°C after photo-lithography showed a very high pH sensitivity and good linearity, so we use best parameters to fabricate urea biosensor.



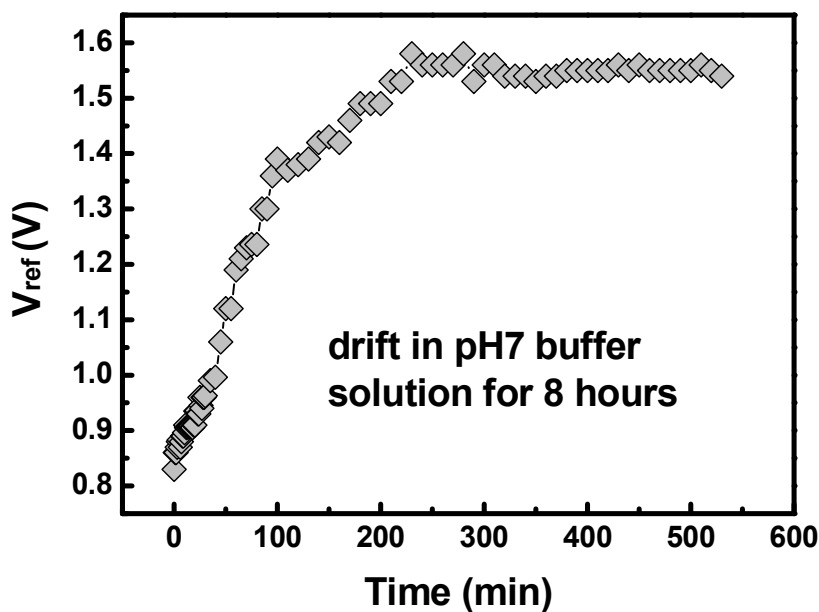
4.5 The drift phenomenon to pH buffer solution

The phenomena of dispersive transport can be found in a broad class of disordered materials. Regarding to the signal drifting issue, the drift rate of pH-ISFET is described using a hopping and/or trap-limited transport mechanism, also known as dispersive transport [4, 5], to evaluate the hydration rate of the insulator. In an amorphous material, for example, dispersive transport may arise from hopping motion through localized states (hopping transport), trap-limited transport in the presence of traps possessing an exponential energy distribution (multiple-trap transport), or a combination of the aforementioned transport mechanisms (trap-controlled hopping transport) [6].

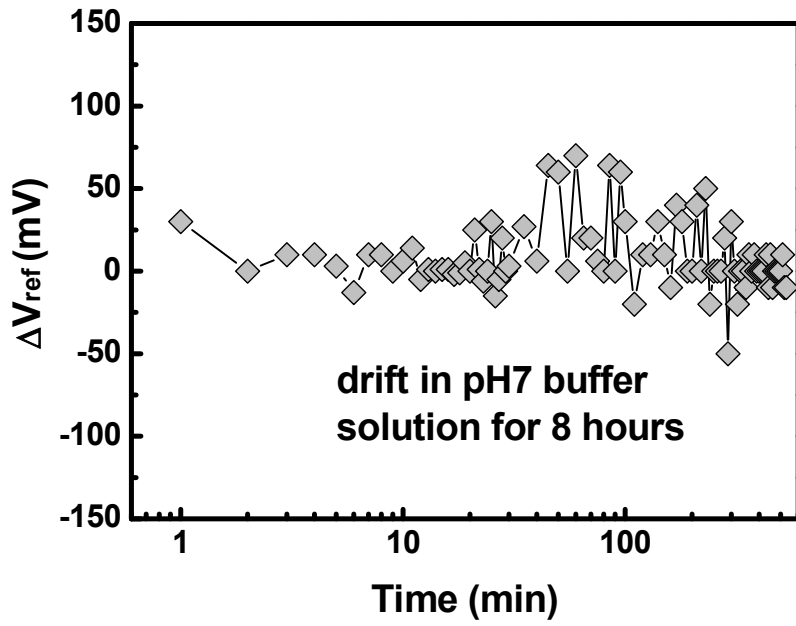
Dispersive transport causes decay in the density of sites/traps occupied by the species going through transport [7]. The hypothesis that hydration of the gate dielectric is controlled by a dispersive transport mechanism is sustained by the presence of buried

surface sites and/or the presence of traps (specifically electrically active silicon dangling bonds). The variations in the chemical composition of the insulator surface leads to the change in number of surface site with time, thus causing a monotonic temporal increase in the threshold voltage. In this study, the drift rate of the ZrO_2 sensing membrane after different annealing temperature treatments was evaluated after submerging the devices in a pH 7 standard solution for 8 h.

Figure 4-17 and 4-18 are time to drift in pH7 buffer solution of EIS capacitors for 8 hours (annealing at $350^\circ C$ and $450^\circ C$). In this result, the drift voltage of EIS capacitor after annealed at $350^\circ C$ was 0.72 V, and the drift voltage of EIS capacitor after annealed at $450^\circ C$ was 0.01 V. Then we could estimate the drift rate for $350^\circ C$ was about 114 mV/h, the drift rate for $450^\circ C$ was about 18 mV/h. The EIS capacitor which annealed at $450^\circ C$ showed better drift character. As a result of that, extrinsic ions can neutralize and compensate these defects (dangling bonds). However, a higher drift rate was considered to be caused by the formation of a silicate layer producing the presence of buried surface sites and/or traps [8].

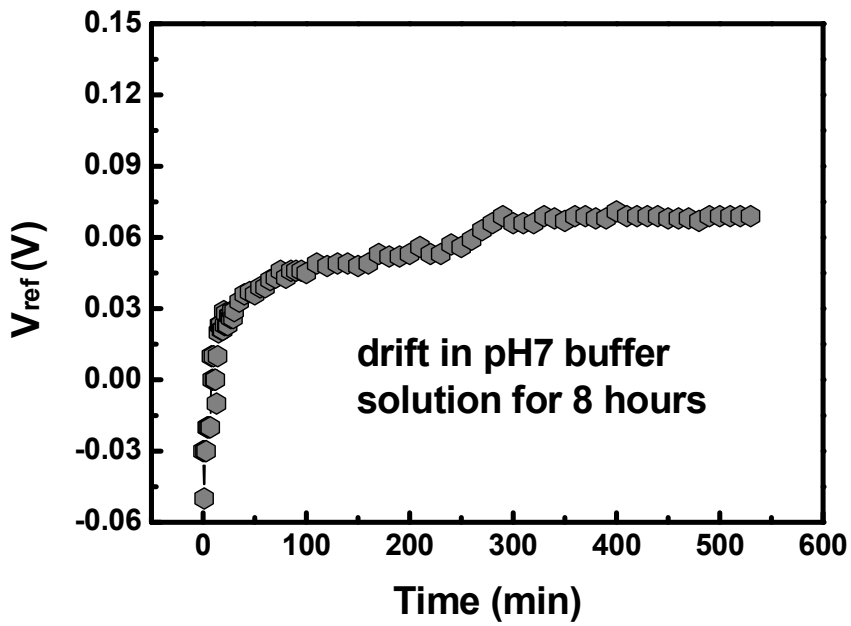
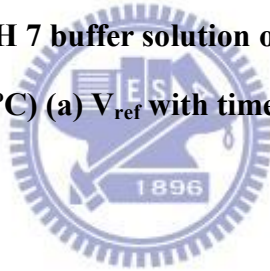


(a)

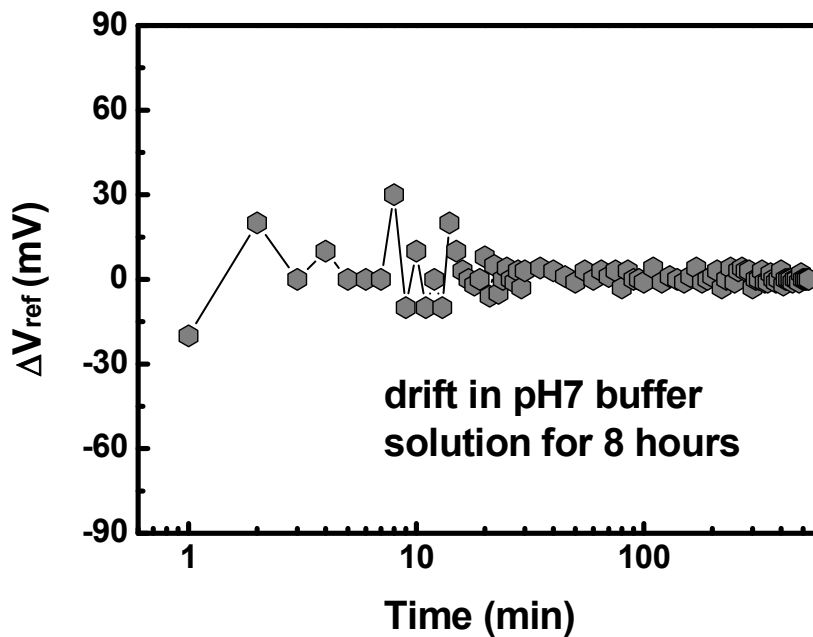


(b)

Figure 4-17 Time to drift in pH 7 buffer solution of EIS capacitor for 8 hours (annealing at 350°C) (a) V_{ref} with time, (b) ΔV_{ref} with time



(a)



(b)

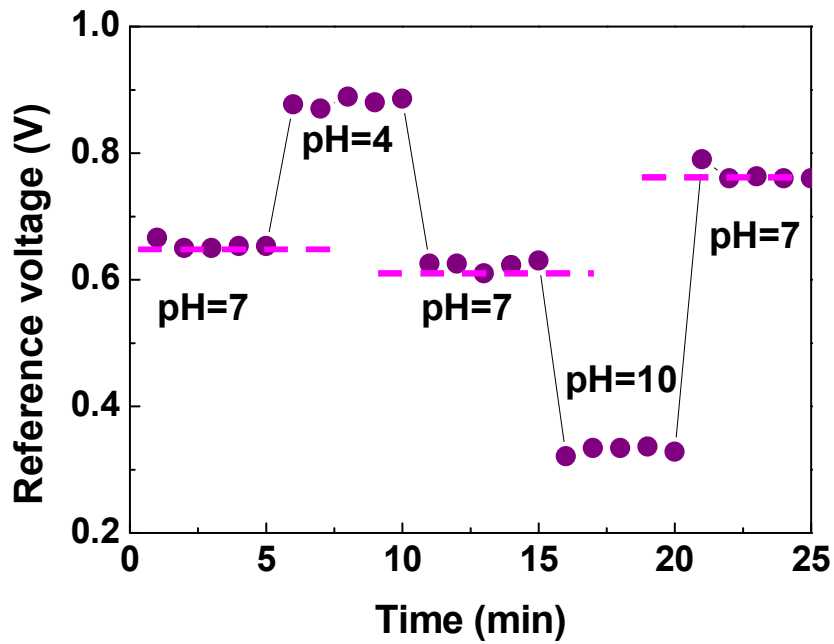
Figure 4-18 Time to drift in pH 7 buffer solution of EIS capacitor for 8 hours (annealing at 450°C) (a) V_{ref} with time, (b) ΔV_{ref} with time

4.6 The influence on the hysteresis

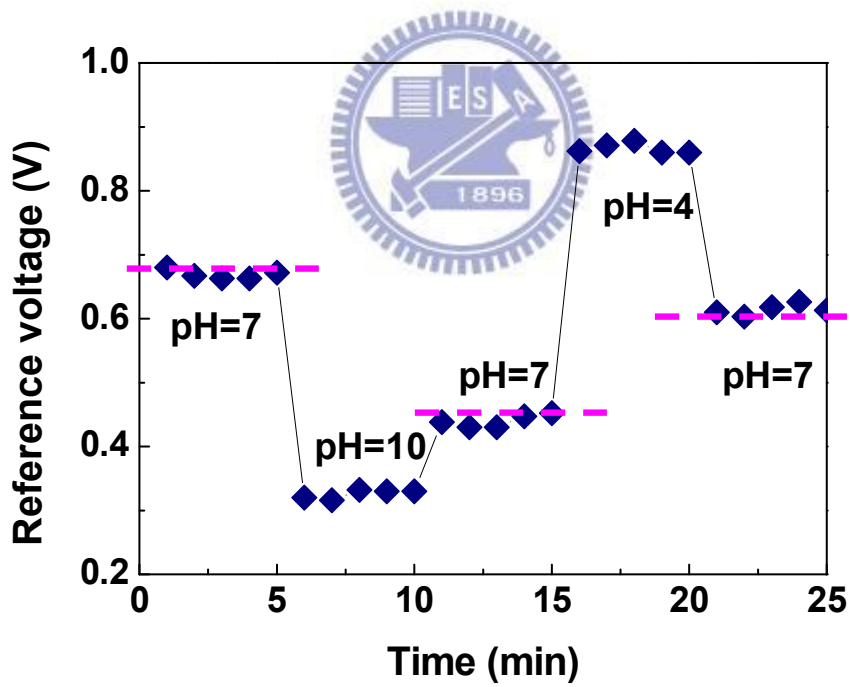
In EIS based pH sensing, the hysteresis phenomenon could be due to the defects of a dielectric film, resulting in the formation of porous structures. The interior sites of these porous defects could react with the ions existing in the tested solution and thus causes hysteresis response. Another possible cause is the interaction of ions in the solution with the responding sites along the boundaries of grains on an insulator film [8]. In this work, the hysteresis of pH sensing of the proposed EIS devices with varied ZrO_2 thin layers studied were evaluated directly by immersing the prepared sensors in each pH standard solution for up to 5 min in the set cycle of pH 7→4→7→10→7 and 7→10→7→4→7. The hysteresis voltage discussed here is defined as the gate voltage difference between the initial and terminal voltages measured in the above cycle. Fig. 4-19 and 4-20 showed

the profiles of the evaluation in the set cycle of pH 7→4→7→10→7 and 7→10→7→4→7, respectively. It can be found from the results that the hysteresis voltage of EIS device with the ZrO₂ sensing film prepared at 450°C showed the lowest value of 0.13V and 0.08V for the pH loop of 7→10→7→4→7, respectively within the experimental conditions investigated. This could be due to the formation of a thinner Zr-silicate interfacial layer and a rougher surface, accordingly leading to the formation of smaller number of interior sites occurred in the 450°C case.

Conversely, the EIS device with ZrO₂ sensing film annealed at 350°C exhibited the highest hysteresis voltage of 0.22 V and 0.17 V in the pH loops of pH 7→10→7→4→7, respectively. All these results again demonstrated the reasonable reproducibility of detections by the proposed ZrO₂-based EIS devices. Particularly, ZrO₂-based EIS devices annealed 450°C exhibited the optimum reproducibility of detection within the experimental conditions explored. In addition, the H⁺ ions diffused from buried sites in acidic solution, whereas HO⁻ ions diffused from buried sites in alkaline solution. The rate of diffusion of H⁺ ions was faster than that of the HO⁻ ions because of their smaller size. Therefore, the hysteresis in the acid solutions was smaller than that in the alkaline solutions. So we observed hysteresis voltage in the pH loops of pH 7→10→7 was higher than in the pH loops of pH 7→4→7.



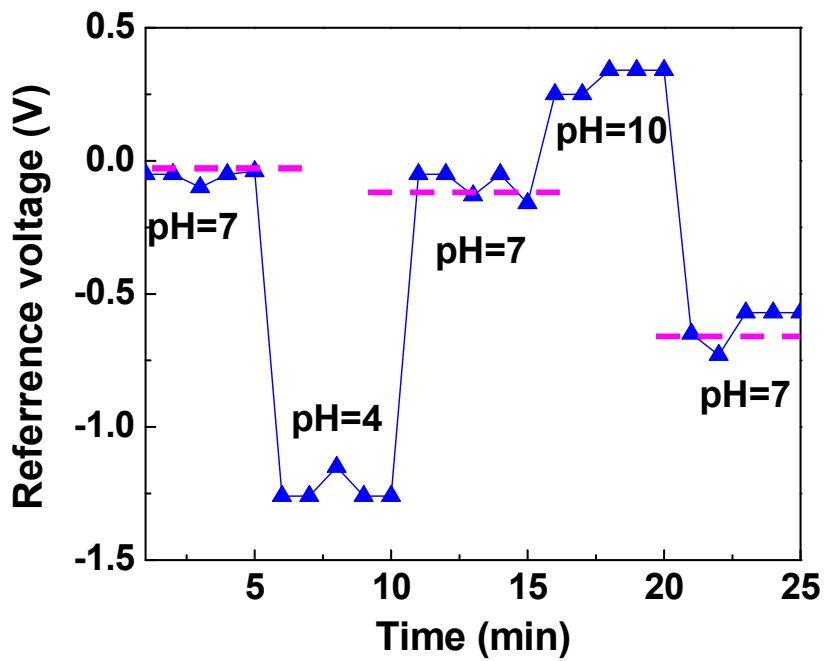
(a)



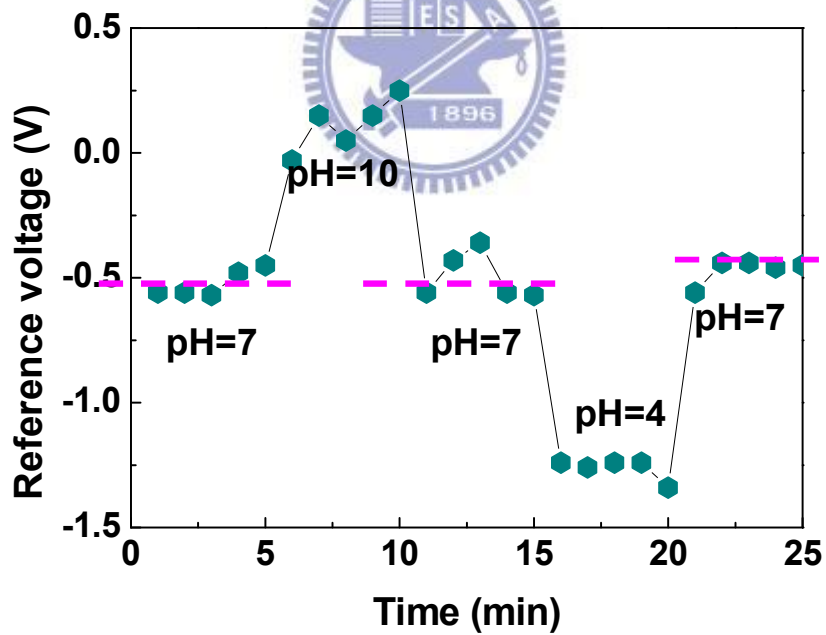
(b)

Figure 4-19 Hysteresis phenomenon to time of EIS capacitor (annealing at 350°C)

(a) pH 7→4→7→10→7, (b) pH 7→10→7→4→7



(a)



(b)

Figure 4-20 Hysteresis phenomenon to time of EIS capacitor (annealing at 450°C)

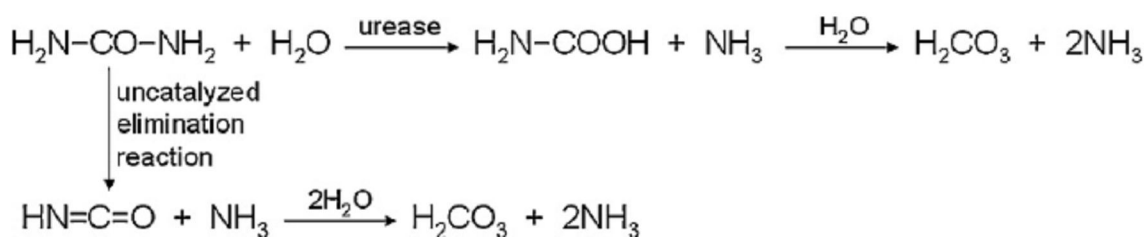
(a) pH 7 → 4 → 7 → 10 → 7, (b) pH 7 → 10 → 7 → 4 → 7

Annealing temperature	pH 7→4→7→10→7		pH 7→10→7→4→7	
	pH 7-4-7	pH 7-10-7	pH 7-10-7	pH 7-4-7
350°C	0.03 V	0.13 V	0.22 V	0.17 V
450°C	0.09 V	0.42 V	0.13 V	0.08 V

Table 4-2 Hysteresis phenomenon to time of EIS capacitor at different annealing temperature

4.7 Demonstration case for urea biosensor

Ureases (urea amidohydrolases, EC 3.5.1.5) are a group of enzymes widespread in nature among plants, bacteria, fungi, algae and invertebrates that, although with different protein structures, exercise a single catalytic function, that is the hydrolysis of urea, its final products being ammonia and carbonic acid. Deceptively simple, this function is frequently looked at as a response of nature to the ubiquitous presence of urea. Functionally, ureases belong to the superfamily of amidohydrolases and phosphotriestrases [10]. The primary common feature of the enzymes is the presence of metal centers in their active sites, whose task is to activate the substrate and water for the reaction.



In urease-catalyzed hydrolysis of urea, the two protagonists of the reaction, urea and

urease are special in the development of natural sciences [11]. Figure 4-21 is catalytic domain of urease in different amounts of urea [12].

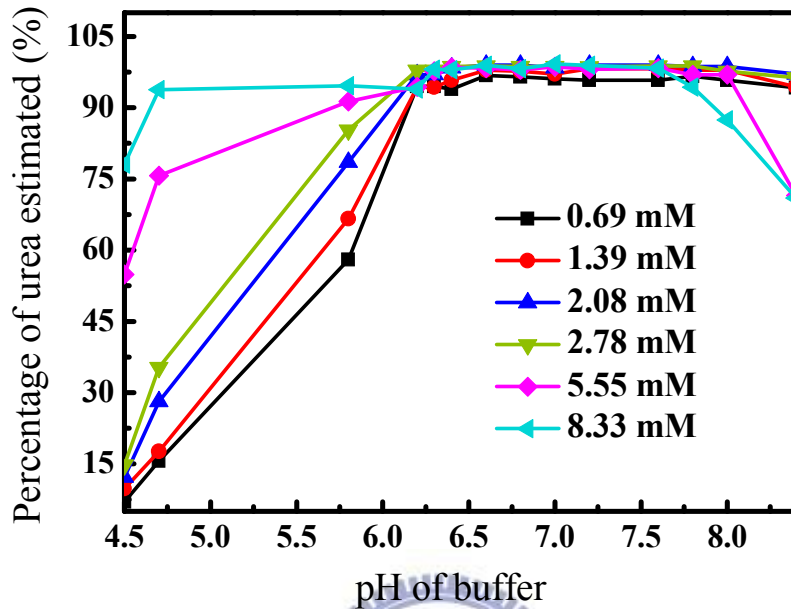


Figure 4-21 Efficiency of hydrolysis at variable buffer pH values (different amounts of urea)

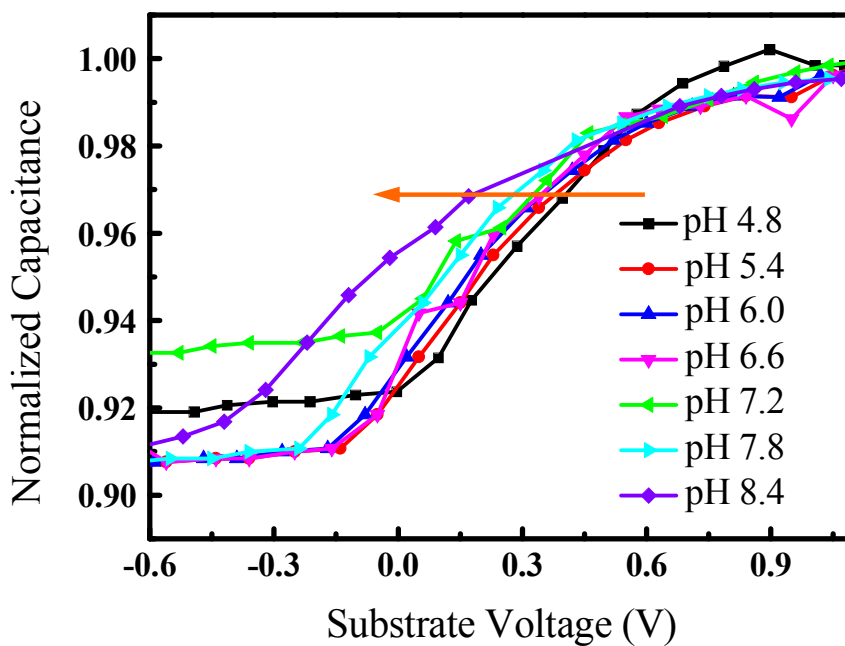


Figure 4-22 Normalized C-V curves of ZrO_2 to EIS capacitor (from pH 4.8 to 8.4)

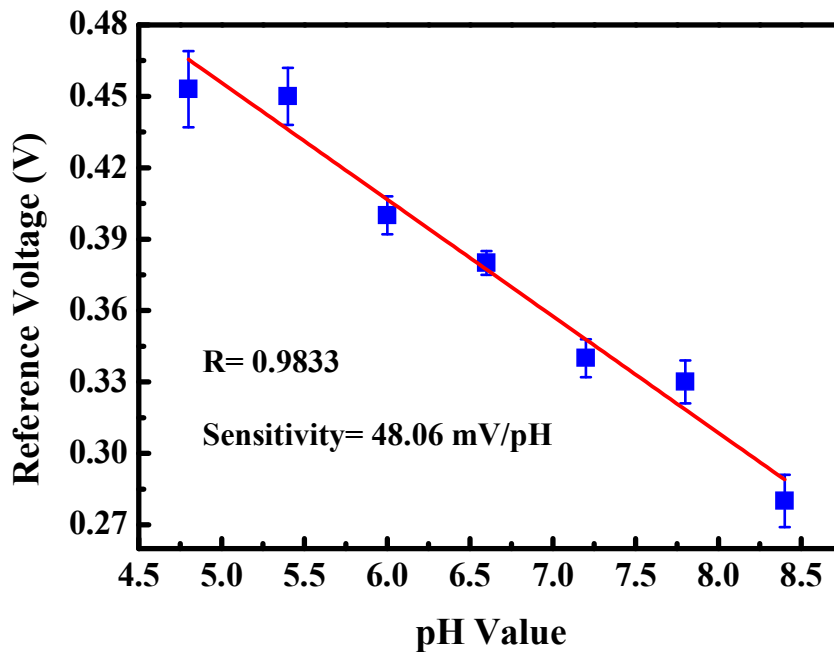


Figure 4-23 Sensitivity characteristic of a ZrO₂ EIS capacitor (from pH 4.8 to 8.4)

For detailed pH sensitivity in catalytic domain of urease, we measured C-V curves of ZrO₂ to EIS capacitor (from pH 4.8 to 8.4) as shown in figure 4-22, 4-23. Urease catalyzes the hydrolysis of urea to ammonium, hydroxyl, and bicarbonate ions. The increase in the HO⁻ ion concentration produces a potential change at the electrode surface that is proportional to the urea concentration. We prepared an enzymatic EIS-based urea biosensor from these devices, using urease as the biocomponent. At first, we use ZrO₂ EIS capacitor to do blank experiment toward various urea concentrations. The results are in figure 4-24, 4-25, we observe that EIS structure with ZrO₂ sensing film had sensitivity of urea. The C-V curves were shifted in different concentration of urea. In order to prove the shift was not because of pH value changed, we used pH meter to measure the pH values of urea solutions as shown in table 4-3. The pH value just added 0.13, but the shift of C-V curves was 1.01 V. It is found that the presented device was able to detect urea with good linearity (R= 0.9958) and reasonable sensitivity of 27.29

mV/mM in the urea concentration range of 3 to 40 mM, which is sufficient for general clinical examination of blood urea.

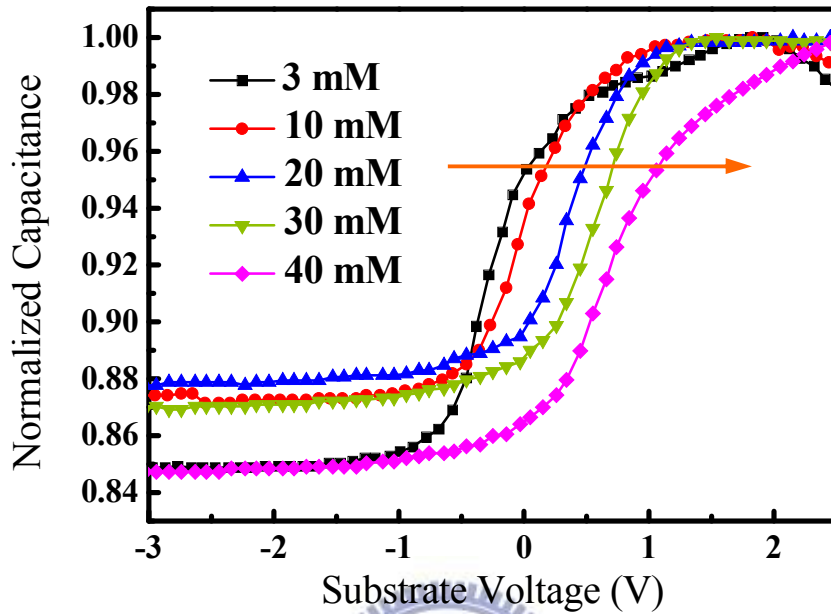


Figure 4-24 Normalized C-V curves of a ZrO₂ EIS capacitor (annealing at 450°C) toward various urea concentrations

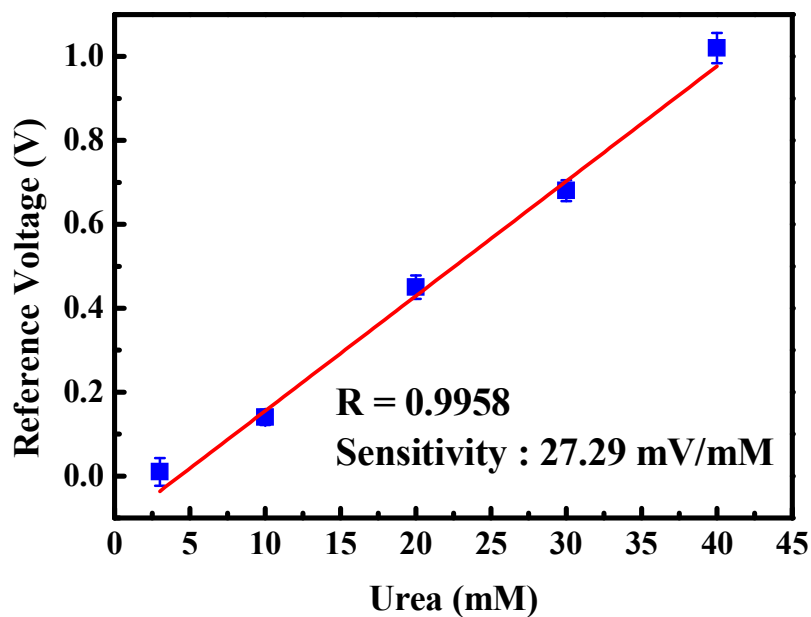


Figure 4-25 Sensitivity characteristic of a ZrO₂ EIS capacitor (annealing at 450°C) toward various urea concentrations

C_{urea}	3 mM	10 mM	20 mM	30 mM	40 mM
pH	7.80	7.86	7.90	7.91	7.93

Table 4-3 The pH values of urea solutions (from 3 mM to 40 mM in pH 7 buffer solutions)

Then we study the urea sensitivity of EIS capacitor which immobilized urease by entrapment method. The sensor is virtually configured by combining pH-EIS mechanism with an enzyme-immobilized film as aforementioned. The principle of sensing is based on the detection of pH alteration caused by the specific enzyme–substrate reaction. For the biosensing of this kind, the sensing performance of the pH-EIS mechanism is crucially important. Consequently, ZrO₂ sensing membrane fabricated at the annealing temperature of 450°C, previously proved to have better pH sensing performance, was adopted in this application. In this work, a urea biosensor with a hybrid structure of urease-containing alginate film/ZrO₂ membrane/p-Si EIS was constructed. The performances of biosensors of this kind are largely dependent on the enzyme immobilization approaches, which refers to fixing enzyme molecules on a transducer for biorecognition purpose. Because of immobilize with urease, the detection of urea biosensor was aimed at the products after enzyme reacted. Figure 4-26, 4-27 are the characteristic of this urea biosensor which immobilized urease. It is found that the presented device was able to detect urea with reasonable sensitivity of 6.22 mV/mM in the urea concentration range of 3 to 40mM. We think the different shift of C-V curves and sensitivity is because of variety ions in solution which change the surface potential of sensing film.

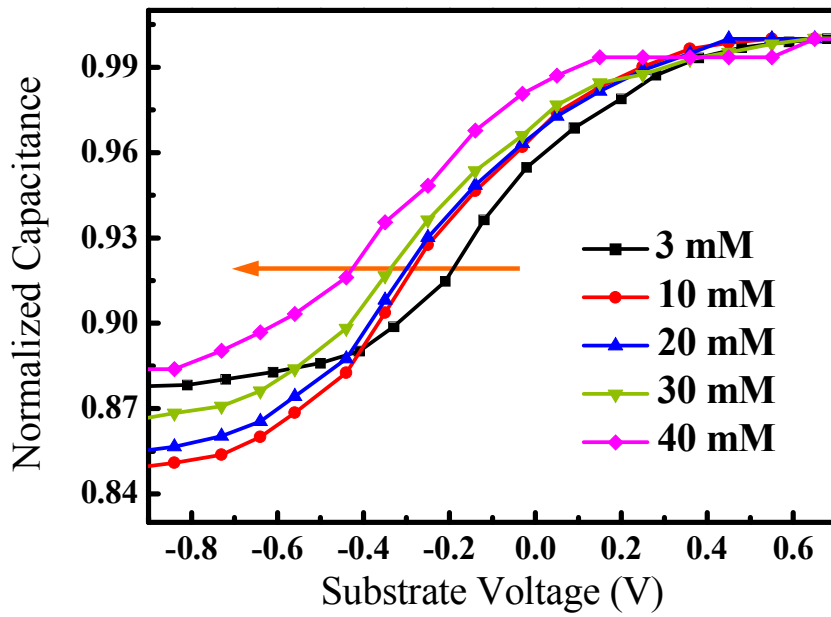


Figure 4-26 Normalized C-V curves of ZrO_2 which immobilized urease to urea biosensor (annealing at $450^\circ C$)

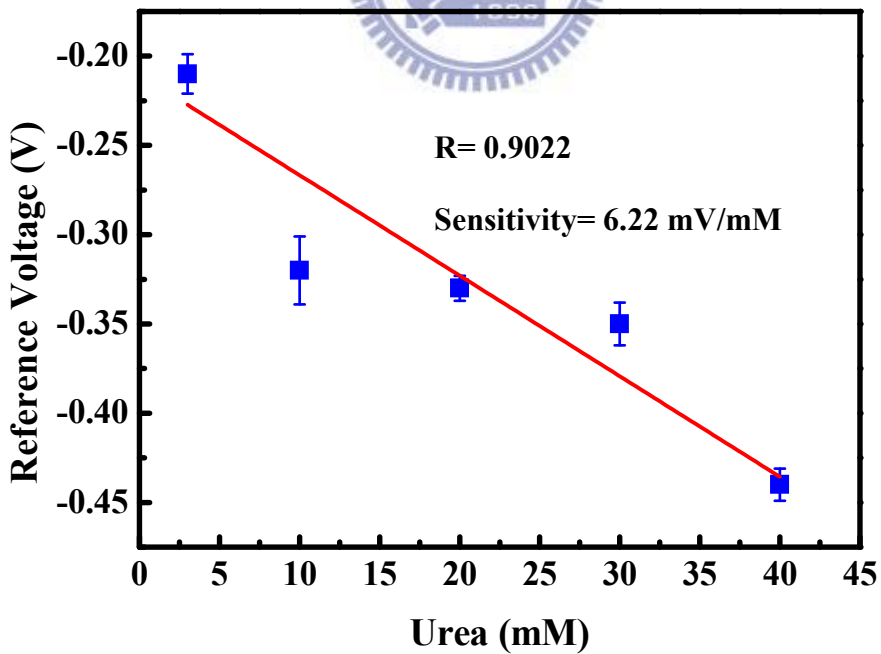


Figure 4-27 Sensitivity characteristic of ZrO_2 which immobilized urease to urea biosensor (annealing at $450^\circ C$)

C_{urea}	3 mM	10 mM	20 mM	30 mM	40 mM
pH	7.06	7.09	7.12	7.15	7.17

Table 4-4 The pH values of urea solutions after catalyzed by urease (from 3 mM to 40 mM in pH 7 buffer solutions)

We also detected the pH values of urea solutions after catalyzed by urease as shown in table 4-4. The difference in pH value between 3 mM and 40 mM was 0.13, and all solutions were weak base. This result could be connected with the products after catalyzed by urease — H_2CO_3 and NH_3 . When the reaction of urease was finished, an equivalent H_2CO_3 of and two equivalents of NH_3 would be produced. They would be dissociated in pH7 buffer solution until attain equilibrium. According to the dissociation properties, the $\text{p}K_{\text{a}1}$ and $\text{p}K_{\text{a}2}$ values of H_2CO_3 are 6.36 and 10.25, the $\text{p}K_{\text{b}}$ value of NH_3 is 4.75. NH_3 has higher equilibrium constant of base and two equivalents of product, so caused the solutions become weak base.

4.7.1 Summary

For the study of urea biosensor, we first understand the catalytic domain of urease in different amounts of urea and then measure the sensing property of ZrO_2 EIS capacitor in this pH region. In this work, a urea biosensor with a hybrid structure of urease-containing alginate film/ ZrO_2 membrane/Si-sub EIS was constructed. The enzyme immobilization by gel entrapment method was adopted to immobilize the enzyme molecules onto ZrO_2 sensing membrane in this case, providing a relatively milder condition to possibly

minimize the loss of enzyme activity during immobilization process. It is found that the EIS capacitor and presented device which immobilized urease were able to detect urea with good linearity and reasonable sensitivity in the urea concentration range of 3 to 40mM, which is sufficient for general clinical examination of blood urea. The observation suggests that EIS capacitor can sense the electrolyte of urea, and the device which immobilized urease can sense the electrolyte of H_2CO_3 and NH_3 .

4.8 Conclusions

The sol-gel process is infrequent to be used in ISFET. Compared with conventional process (such as sputter and PECVD), there are much more impact terms in the sol-gel process: solvent, concentration, spin-coating, O_2 plasma, annealing temperature and time. In this study, we found better parameters in the fabrication of ZrO_2 EIS capacitor. Considering non-ideal phenomena such as the drift may cause the gate voltage shift, if the driving current is too small that the gate voltage may dominate it. According to the Eq. (2-3), to increase the driving current such as decrease channel length, increase the mobility or use high-k material to increase the capacitance, these ways may decrease the influence on the drift to pH-ISFET.

Make a study of another non-ideal phenomena, the hysteresis effect in ZrO_2 EIS capacitor by the sol-gel process is much obvious than the conventional pH-ISFET. It must because the sensing film by the sol-gel method is not very dense and firm. There are some traps in ZrO_2 structure, so they possibly affect the ion distribution. This method succeeds in make high-k ZrO_2 film and EIS capacitor, but still has some characteristic can be improved.

By analyze structure properties, pH sensitivity and non-ideal phenomena, we chose EIS capacitor which annealing at 450°C to demonstrate urea biosensor. We observed the

EIS capacitor with ZrO_2 sensing film has sensitivity of urea in pH buffer solution. Then we also immobilized urease on ZrO_2 sensing film to detect the urea sensitivity after urease react. There are two different mechanisms in urea biosensors.

4.9 References

- [1] H. C. You, T. F. Lei, F. H. Ko, Application of novel lithography and nano-crystal technique in the fabrication of nano-devices and memories, (2006).
- [2] M. Houssa, High- k Gate Dielectrics, Institute of Physics, London (2004).
- [3] T. Mori, H. Hoshino, Y. Ishikawa, Preparation of high purity $ZrSiO_4$ powder using sol-gel processing and mechanical properties of the sintered body, Journal of the American Ceramic Society 75 (1992) 2420-2426.
- [4] H. Scher, E. W. Montroll, Anomalous transit-time dispersion in amorphous solids Physical Review B 12 (1975) 2455-2477.
- [5] G. Pfister, H. Scher, Time-dependent electrical transport in amorphous solids: As_2Se_3 , Physical Review B 15 (1977) 2062-2083.
- [6] S. Jamasb, S. Collins, R. L. Smith, A physical model for drift in pH ISFETs, Sensors and Actuators B 49 (1998) 146-155.
- [7] J. Kakalios, R. A. Street, W. B. Jackson, Stretched-exponential relaxation arising from dispersive diffusion of hydrogen in amorphous silicon, Physical Review Letters 59 (1987) 1037-1040.
- [8] M. H. Wua, C. H. Cheng, C. S. Lai, T. M. Pan, Structural properties and sensing performance of high- k Sm_2O_3 membrane-based electrolyte-insulator-semiconductor for pH and urea detection, Sensors and Actuators B 138 (2009) 221-227.
- [9] L. Bousse, H. H. van der Vlekkert, N. F. de Rooij, Hysteresis in Al_2O_3 -gate ISFETs, Sensors and Actuators B 2 (1990) 103-110.

- [10] L. Holm, C. Sander, An evolutionary treasure: unification of a broad set of amidohydrolases related to urease, *Proteins* 28 (1997) 72–82.
- [11] B. Krajewska, Ureases I. Functional, catalytic and kinetic properties: A review, *Journal of Molecular Catalysis B: Enzymatic* 59 (2009) 9–21.
- [12] W. W. Kay, M. A. H. Reid, The optimum buffer pH for hydrolysis of urea by urease, *Biochemical Journal* 28 (1934) 1798-1801.



Chapter 5

Future Work

5.1 Future work

In our experiment, sensitivity of EIS structure with ZrO_2 deposited by the sol-gel process and urea biosensor are studied. And, we have also try to simplify the procedure of fabrication of biosensor by extend gate electrode and use of SPE. Based on the observed result, we have found out Ag-SPE is a good candidate for ISFET and solid-state reference electrode. When in experiment of pH sensitivity, the performance sometimes will fail and unstable during measurement especially in $pH \leq 4$ and $pH \geq 10$. The sol-gel-derived sample has lower precision and reliability than the conventional sample. So, the optimized sol-gel method, including the influence of solvent, annealing temperature, and the accurate thickness of SiO_2 and ZrO_2 , needs to be studied further. The mechanism of urea biosensor is also need to be understood more in detail study.

簡 歷

姓 名：邱 品 樺

性 別：女

出生日期：民國 74 年 02 月 21 日

籍 貫：台灣省高雄縣

學 歷：國立高雄師範大學化學系

國立交通大學材料科學與工程學系奈米科技碩士班

碩士論文：以溶膠－凝膠法製作二氧化鋯感測層在電解質－絕緣層－

半導體結構對pH及尿素生物感測之研究

The study of sol-gel-derived ZrO₂ sensing film based on electrolyte-insulator-semiconductor for pH detection and urea biosensing